



UNIVERSIDADE DE SÃO PAULO
FACULDADE DE CIÊNCIAS FARMACÊUTICAS DE RIBEIRÃO PRETO

**Fragment screening against *Schistosoma mansoni*
dihydroorotate dehydrogenase: a modern approach for drug
discovery**

**Busca de ligantes para a diidroorotato desidrogenase: uma
abordagem moderna para descoberta de drogas**

RENAN MININ DE MORI

Ribeirão Preto
2021

UNIVERSIDADE DE SÃO PAULO
FACULDADE DE CIÊNCIAS FARMACÊUTICAS DE RIBEIRÃO PRETO

RENAN MININ DE MORI

Fragment screening against *Schistosoma mansoni* dihydroorotate dehydrogenase: a modern approach for drug discovery

Busca de ligantes para a diidroorotato desidrogenase: uma abordagem moderna para descoberta de drogas

Master dissertation presented to the Graduate Program of School of Pharmaceutical Sciences of Ribeirão Preto/USP for the degree of Master in Sciences.

Concentration Area: Chemistry and Biological Physics

Supervisor: Profa. Dra. Maria Cristina Nonato

Corrected version of a master dissertation presented to the Pharmaceutical Sciences Graduate Program, on 04/06/2021. The original version is available at School of Pharmaceutical Sciences of Ribeirão Preto /USP.

Ribeirão Preto
2021

MORI, R. M.	Fragment screening against <i>Schistosoma mansoni</i> dihydroorotate dehydrogenase: a modern approach for drug discovery		MESTRADO FCFRPUSP 2021
-------------	---	--	------------------------------

I AUTHORIZE THE REPRODUCTION AND TOTAL OR PARTIAL DISCLOSURE OF THIS WORK, BY ANY CONVENTIONAL OR ELECTRONIC MEANS

De Mori, Renan Minin

Fragment screening against *Schistosoma mansoni* dihydroorotate dehydrogenase: a modern approach for drug discovery. Ribeirão Preto, 2021.

67 p.; 30 cm.

Master dissertation presented to the Graduate Program of School of Pharmaceutical Sciences of Ribeirão Preto/USP for the degree of Master in Sciences. Concentration Area: Chemical and Biological Physics

Supervisor: Nonato, Maria Cristina

1. Fragment screening; 2. *Schistosoma mansoni* dihydroorotate dehydrogenase (*SmDHODH*); 3. Crystallography; 4. Schistosomiasis; 5. *Schistosoma mansoni*.

APPROVAL PAGE

Renan Minin de Mori

Fragment screening against *Schistosoma mansoni* dihydroorotate dehydrogenase: a modern approach for drug discovery.

Master dissertation presented to the Graduate Program of School of Pharmaceutical Sciences of Ribeirão Preto/USP for the degree of Master in Sciences.

Concentration Area: Chemistry and Biological Physics

Supervisor: Prof. Dr. Maria Cristina Nonato

Approved on:

Examiners

Prof. Dr. _____

Institution: _____ Signature: _____

Prof. Dr. _____

Institution: _____ Signature: _____

Prof. Dr. _____

Institution: _____ Signature: _____

Inscription

Aos meus avós, que não puderam estar comigo ao longo da minha vida acadêmica,
mas que tenho certeza de que estariam felizes com as minhas conquistas.

Acknowledgements

Primeiramente, gostaria de agradecer a Deus por ter me dado sabedoria em cada passo do meu caminho, por ter me guiado e me auxiliado a passar pelos pontos de inflexão da minha vida, que irão me levar, sem dúvida, para mais perto do seu propósito.

Agradeço aos meus pais (Vladimir e Sirlene), pois, sem eles, nenhum objetivo que já foi atingido, ou que ainda será, seria possível. Agradeço a todos os sacrifícios feitos ao longo dos anos para me propiciarem uma formação acadêmica, e por formarem meu caráter.

Aos meus tios (Alfredo e Sandra), que são como segundos pais para mim e que sempre, mesmo de longe, apoiaram-me na minha jornada.

À minha namorada (Virgínia), que mudou meu jeito de ver o mundo, e foi essencial ao longo do meu mestrado com todo seu carinho.

Agradeço à minha orientadora Profa. Maria Cristina Nonato por ter me aceitado em seu laboratório, apesar de ter vindo de uma área completamente diferente, e por ter me dado uma “bagagem” científica imensa durante esses dois anos. Algo que jamais poderei retribuir à altura.

Ao Prof. Flávio Emery, que, juntamente com o seu laboratório, foi essencial em todo o desenvolvimento do meu projeto de pesquisa.

Agradeço o apoio e suporte dos meus amigos do LCP-RP, tanto cientificamente quanto pessoalmente. Mais que colegas de trabalho, vocês serão para sempre meus amigos.

Agradeço também à FCFRP e à Universidade de São Paulo pelo apoio técnico e institucional que proporcionaram o desenvolvimento do meu projeto.

À Fundação de Amparo a Pesquisa do Estado de São Paulo (FAPESP, processo nº 2019/04395-6) e ao Conselho Nacional de Desenvolvimento Tecnológico e Científico (CNPq, processo nº 132112/2019-1) pelo suporte financeiro.

À John Wiley & Sons por permitir o uso do artigo “Structural basis for the function and inhibition of dihydroorotate dehydrogenase from *Schistosoma mansoni*”. License number: 5016010292565.

O presente trabalho foi realizado com apoio da Coordenação de Aperfeiçoamento de Pessoal de Nível Superior – Brasil (CAPES) – Código de Financiamento 001.

“It’s impossible to map out a route to your destination if you don’t know where you’re starting from.”

Suze Orman

Abstract

Mori, R.M. **Fragment screening against *Schistosoma mansoni* dihydroorotate dehydrogenase: a modern approach for drug discovery.** 2021. 67p. Dissertation (Master). Faculdade de Ciências Farmacêuticas de Ribeirão Preto – Universidade de São Paulo, Ribeirão Preto, 2021.

Prevalent in tropical and subtropical areas, schistosomiasis is a serious public health problem, especially in rural and poor communities without access to adequate sanitation and safe drinking water, being one of the most prevalent neglected tropical diseases (NTDs). Transmission has been reported in dozens of countries with 52 considered endemic regions. Its control, over the past 30 years, depends on a single drug, praziquantel. Its mechanism of action is not fully understood and displays considerable drawbacks. Therefore, the development of an alternative treatment for schistosomiasis is unquestionably urgent. In the last decades, due to the advance of recombinant DNA and gene technologies, the use of target-based drug discovery (TDD) has increased significantly. Our work has focused on exploiting TDD strategies to develop new therapeutics to treat schistosomiasis, mainly based on the use of fragment screening. By using compounds of low molecular weight, fragment screening has appeared as an important strategy in the pipeline of drug discovery. Fragments can cover a broader range of the chemical space with fewer compounds, often binding with better ligand efficiencies than traditional screening. With this, hits are generally able of binding to a higher number of proteins than conventional 'drug-size' molecules. We were interested in evaluating the enzyme dihydroorotate dehydrogenase (DHODH) as a drug target against schistosomiasis. DHODH is a flavoenzyme that catalyzes the stereospecific oxidation of (S)-dihydroorotate (DHO) to orotate during the fourth and only redox step of the *de novo* pyrimidine nucleotide biosynthetic pathway, laying at the center of critical biochemical pathways. DHODH has been considered an important drug target for cancer, autoimmune and parasitic diseases, among other infections. In collaboration with Prof. Flávio Emery's laboratory, we screened several fragments against the *Schistosoma mansoni* DHODH (*SmDHODH*) through the use of structural, biophysical, and enzymatic assays, and identified potent and selective inhibitors against *SmDHODH* in the nanomolar range. We also reported here the first crystal structure of *SmDHODH* in complex with an atovaquone analogue inhibitor (PDB: 6UY4). Our structural studies have shown: (a) the open conformation of the active site loop in a class 2 DHODH; (b) the presence of a protuberant domain, only noticed for *Schistosoma* spp. DHODHs, that could modulate and control the inhibitor binding site; (c) a detailed description of an unexpected binding mode for the atovaquone analogue to *SmDHODH*. With this, our work reveals key molecular interactions required for the activity of atovaquone and its analogues, and presents the basis for fragments optimization that could guide future drug design strategies in the fight against schistosomiasis.

Keywords: Fragment screening; *Schistosoma mansoni* dihydroorotate dehydrogenase (*SmDHODH*); Crystallography; Schistosomiasis; *Schistosoma mansoni*.

Resumo

Mori, R.M. **Busca de ligantes para a diidroorotato desidrogenase: uma abordagem moderna para descoberta de drogas.** 2021. 67f. Dissertação (Mestrado). Faculdade de Ciências Farmacêuticas de Ribeirão Preto – Universidade de São Paulo, Ribeirão Preto, 2021.

Prevalente em áreas tropicais e subtropicais, a esquistossomose é um grave problema de saúde pública, especialmente em comunidades rurais e pobres sem acesso a saneamento e água potável, sendo uma das doenças tropicais negligenciadas (DTNs) mais prevalentes. A transmissão foi reportada em dezenas de países com 52 regiões consideradas endêmicas. Seu controle, nos últimos 30 anos, depende de um único medicamento, o praziquantel. Seu mecanismo de ação não é totalmente compreendido e apresenta desvantagens consideráveis. Portanto, o desenvolvimento de um tratamento alternativo para a esquistossomose é indiscutivelmente urgente. Nas últimas décadas, devido ao avanço das tecnologias de DNA e proteínas recombinantes, o uso da descoberta de fármacos baseadas em alvos aumentou (TDD) significativamente. Nosso trabalho tem se concentrado no uso de estratégias de TDD para o desenvolvimento de novas terapêuticas para o tratamento da esquistossomose, principalmente com base na triagem de fragmentos. Ao usar compostos de baixo peso molecular, a triagem de fragmentos surge como uma estratégia importante no *pipeline* de descoberta de fármacos. Os fragmentos podem cobrir uma faixa mais ampla do espaço químico com menos compostos, muitas vezes ligando-se com melhor eficiência do que a triagem tradicional. Com isso, os *hits* são geralmente capazes de se ligar a um número maior de proteínas do que as moléculas convencionais. Estamos interessados em avaliar a enzima diidroorotato desidrogenase (DHODH) como alvo contra a esquistossomose. A DHODH é uma flavoenzima que catalisa a oxidação estereoespecífica do (S)-diidroorotato (DHO) para orotato durante a quarta e única etapa *redox* da *via de novo* da biossíntese de pirimidinas. A DHODH tem sido considerada um importante alvo para doenças como: câncer, doenças autoimunes e parasitárias, entre outras infecções. Em colaboração com o laboratório do Prof. Flávio Emery, testamos diversos fragmentos contra a DHODH de *Schistosoma mansoni* (*SmDHODH*) através de estudos estruturais, biofísicos e enzimáticos, identificando inibidores potentes e seletivos contra a *SmDHODH* na faixa nanomolar. Também descrevemos aqui a primeira estrutura cristalográfica da *SmDHODH* em complexo com um inibidor análogo da atovaquona (PDB: 6UY4). Nossos estudos estruturais mostraram: (a) uma conformação aberta do loop catalítico do sítio ativo em DHODHs de classe 2; (b) a presença de um domínio protuberante, observado apenas para DHODHs de *Schistosoma* spp., que poderia modular e controlar o sítio de interação do inibidor; (c) uma descrição detalhada de um modo de ligação inesperado para o análogo da atovaquona a *SmDHODH*. Com isso, nosso trabalho revela as principais interações moleculares necessárias para a atividade da atovaquona e seus análogos, bem como, as bases para a otimização dos fragmentos que norteará futuras estratégias de desenho de fármacos no combate à esquistossomose.

Palavras-chave: Varredura por fragmentos; *Schistosoma mansoni* diidroorotato desidrogenase (*SmDHODH*); Cristalografia; Esquistossomose; *Schistosoma mansoni*.

List of Figures

Figure 1: Phenotypic and target-based approaches timeline (extracted from Aulner, 2019 (7))	12
Figure 2: Distribution of schistosomiasis worldwide (Adapted from Map: Distribution of schistosomiasis, worldwide, 2012, WHO, © 2012. Extracted from McManus <i>et. al</i> , 2018 (26)).	16
Figure 3: <i>Schistosoma</i> spp. life cycle scheme. (Extracted from Centers for Disease Control and Prevention (27)).	17
Figure 4: Schistosome worm pair. (Extracted from the Trustees of the Natural History Museum).	17
Figure 5: Ping-pong enzymatic reaction catalyzed by class 2 dihydroorotate dehydrogenases (DHODHs). In the first half, the dihydroorotate (DHO) is oxidized to orotate, accompanied by the reduction of the prosthetic group flavin mononucleotide FMN to FMNH ₂ . In the second part, FMN is re-oxidized (FMNH ₂ is converted to FMN) by the final electron acceptor - ubiquinone (Extracted from Mori, R.M. <i>et al</i> , 2020. (56)).	20
Figure 6: Sequence alignment of selected class 2 DHODHs: <i>Sm</i> DHODH (<i>Schistosoma mansoni</i> DHODH; UniProt entry: G4VFD7), <i>Sh</i> DHODH (<i>Schistosoma haematobium</i> DHODH; UniProt entry: A0A094ZN75), <i>Sj</i> DHODH (<i>Schistosoma japonicum</i> DHODH; UniProt entry: Q5DD85), <i>Rn</i> DHODH (<i>Rattus norvegicus</i> DHODH; UniProt entry: Q63707), <i>Pf</i> DHODH (<i>Plasmodium falciparum</i> DHODH; UniProt entry: Q08210), <i>Mt</i> DHODH (<i>Mycobacterium tuberculosis</i> DHODH; UniProt entry: P9WHL1) and <i>Hs</i> DHODH (Human DHODH; UniProt entry: Q02127). Residues that interact with 0230 are indicated by red arrows, and those that interact with the glycerol by black arrows. Residues that vary between <i>Hs</i> DHODH and <i>Sm</i> DHODH along the binding channel are indicated by blue arrows. Residues that interact with the 0230 and vary along the pocket are indicated by pink arrows. The protuberant region (Gly ²⁸⁵ – Lys ²⁹⁴) is highlighted yellow for the <i>Schistosoma</i> spp., and the catalytic loop (Asn ²⁰⁰ – Lys ²¹⁵) in green. The alignment was performed using MULTALIN (69) and graphically displayed using ESPript 3.0 (70). (Extracted from Mori,R.M. <i>et al.</i> , 2020 (56)).	22
Figure 7: Two-dimensional structure representation of the compounds donated by Professor Flávio Emery's laboratory and tested against <i>Sm</i> DHODH by ThermoFMN, enzymatic inhibition and crystallization assays. The IC ₅₀ values (µM) were obtained for the compounds 0009; 0011; 0034; 0230; 0297 and 0320.	28
Figure 8: Two-dimensional structure representation of atovaquone-based compound library evaluated as <i>Sm</i> DHODH-inhibitors (74), and the coenzyme Q ₀ . Compound 1 is teriflunomide, 2 is atovaquone and 3 is brequinar. Compounds 6a to 6k are simplified analogs of atovaquone, classified as 0230-like compounds. Compounds (6l - 6o) were classified as atovaquone-like	

series. Numbers 9 and 10 are 1,4-naphtoquinones derivatives and from 13 to 17 are lapachol derivatives. Compounds 19, 20 and 21 are benzoquinones. (Extracted from Mori, RM. *et al.* (56)).29

Figure 9: SDS-PAGE analysis of nickel affinity chromatography showing the purification steps. M: molecular weight marker. **A:** SmDHODH + 6xHis-SUMO-tag. **B:** Purified protein. 1: Insoluble fraction; 2: Soluble fraction; 3: Flowthrough; 4: Washing step containing 10 mM imidazole; 5: Washing step containing 25 mM imidazole; 6: Protein elution containing 500 mM imidazole; 7: Protein after cleavage; 8: Protein after second affinity chromatography.....32

Figure 10: Two-dimensional structure of atovaquone34

Figure 11: ΔT_m shifts for the tested compounds at 2 mM against SmDHODH from reference of 55.07°C.....35

Figure 12: Fragments tested against SmDHODH. Fragments with positive thermo shifts are colored in blue, those with negative thermo shifts in red, and the fragments classified as neutral in black (no significative deviation). Structural patterns: A) hydroxynaptoquinones, B) furopyridines; C) pyridines; D) carbazole; E) Sulfonamides; F) imidazopyridines and imidazopyrimidines; G) methanocarb; H) aromatics. For compounds 9, 11, 34, 230, 397 and 320 the percentage of inhibition (IC₅₀ in μ M) is presented.....38

Figure 13: A) Pretest of SmDHODH sample in absence of ligands for Micro Scale Thermophoresis (MST). The non-significative variation of the MST profile in the experiment for the pure protein indicates the success in protein labelling. **B)** Binding check for SmDHODH and compound 0320. The MST profile indicates a variation of the relative fluorescence, indicating, a non-homogeneous behavior among the capillaries.40

Figure 14: SmDHODH crystals obtained in A) 0.1 M MES pH 6.5, 1.3 – 1.5 M citrate; and B) 0.1 M HEPES sodium pH 7.5, 1.3 – 1.5M citrate.....41

Figure 15: SmDHODH crystallographic structure represented by cartoon. The central barrel is composed of eight parallel β strands ($\beta_1 - \beta_8$) in lightpink and surrounded by eight α -helices in green ($\alpha_1 - \alpha_8$). The hydrophobic N-terminal domain composed by two α -helices is illustrated in lightblue (α_A and α_B). The catalytic loop (Asn²⁰⁰ – Lys²¹⁵) is highlighted in violet, and the protuberant loop (Gly²⁸⁵ – Lys²⁹⁴) in red. The glycerol molecules, the compound 0230, and the FMN are illustrated by stick models in orange, magenta, and yellow, respectively (Extracted from Mori,R.M. *et al.*, 2020 (56)).43

Figure 16: (A) Superposition between SmDHODH and PfdDHODH (PDB: 1TV5; (88)), HsdDHODH (PDB: 1D3H; (89)), and MtdDHODH (PDB: 4XQ6; not published) showing the catalytic loop conformational rearrangement (Asn²⁰⁰ – Lys²¹⁵). Molecular surface for the SmDHODH is represented in gray. The SmDHODH, HsdDHODH, PfdDHODH, and MtdDHODH catalytic loop is colored in purple, lightblue, palegreen, and lightorange, respectively. The

orotate and FMN are represented by stick models in blue and yellow, respectively. **(B)** *SmDHODH* surface with a glycerol molecule at the entrance of the active site represented as stick model in orange **(C)** Glycerol molecule interactions (Extracted from Mori, R.M. *et al.*, 2020 (56)).44

Figure 17: Circular dichroism spectra for both constructs: full-length (*SmDHODH*) and with the protuberant domain deleted (*SmDHODH Δ loop*), indicating the same secondary structure distribution. The graph represents the molar ellipticity per wavelength, where the full-length construct spectra is represented in black and the Δ loop spectra in red (Extracted from Mori, R.M. *et al.*, 2020 (56)).....46

Figure 18: Graphic of inhibition values vs. ΔT_m shifts for the tested library at 500 μ M against *Schistosoma mansoni* dihydroorotate dehydrogenases: *SmDHODH* (full-length) and *SmDHODH Δ loop*. Reference T_m s are 54.73 °C for *SmDHODH* and 50.4 °C for *SmDHODH Δ loop*. IC_{50} values were extracted from Calil *et al.* (92). (Extracted from Mori, R.M. *et al.* (56)).47

Figure 19: (A) *Schistosoma mansoni* dihydroorotate dehydrogenase (*SmDHODH*; PDBID: 6UY4) molecular surface and cartoon representation. Represented by sticks: 0230 (2-((4-fluorophenyl) amino)-3-hydroxynaphthalene-1,4-dione) in blue, FMN in yellow and glycerol molecules in green. Image created with PyMOL (82). **(B)** Schematic interactions in the complex 0230-*SmDHODH*. C, N, O and F atoms are shown in black, blue, red and lime green, respectively. The green dashed lines represent the hydrogen bonds. Image created with LIGPLOT+ (93). (Extracted from Mori, R.M. *et al.* (56)).49

Figure 20: Schematic interactions in the complex atovaquone-*RnDHODH* (PDID: 1UMM). C, N, O and F atoms are shown in black, blue, red and lime green, respectively. The green dashed lines represent the hydrogen bonds. Image created with LIGPLOT+ (93). (Extracted from Mori, R.M. *et al.* (56)).....51

List of Tables

Table 1: Compounds tested in the initial screening at 200 μM against SmDHODH. Their respective codes and percent of inhibition.....	33
Table 2: IC_{50} values (μM) obtained for SmDHODH against the compounds 0009; 0011; 0034; 0230; 0297 and 0320. *Curve for compound 0012 was not obtained.....	33
Table 3: Data collection and refinement statistics. (Extracted from Mori,R.M. et al. (55)).....	42

List of Equations

Equation 1: Sigmoidal fitting equation used (dose response). Where A1 corresponds to the minimum inhibition value, A2 corresponds to the maximum inhibition value, p corresponds to the Hill slope and LOGx0 corresponds to the inflexion point that correspond to the inflexion point that correspond to the inhibitor concentration responsible for 50% loss of enzymatic activity. 26

List of Abbreviations

ATO	Atovaquone
CD	Circular dichroism
DALY	Disability-adjusted life year
DCIP	Dichlorophenolindophenol
DD	Drug discovery
DEL	DNA encoded library
DHO	Dihydroorotate
DHODH	Dihydroorotate dehydrogenase
DMSO	Dimetilsulfóxido
DSF	Differential scanning fluorimetry
FBLD	Fragment-based lead discovery technique
FMN	Flavin mononucleotide
<i>Hs</i>DHODH	Human dihydroorotate dehydrogenase
HTS	High-throughput-screening
IC₅₀	Half maximal inhibitory concentration
LE	Ligand efficiency
MDA	Mass drug administration
MES	2-(N-morpholino)ethanesulfonic acid
MS	Mass spectrometry
MST	Micro scale thermophoresis
<i>Mt</i>DHODH	<i>Mycobacterium tuberculosis</i> dihydroorotate dehydrogenase
NMR	Nuclear magnetic resonance

NTD	Neglected tropical disease
PDB	Protein Data Bank
PDD	Phenotypic screening
<i>Pf</i>DHODH	<i>Plasmodium falciparum</i> dihydroorotate dehydrogenase
PMSF	Phenylmethanesulfonylfluoride
R&D	Research and development
<i>Rn</i>DHODH	<i>Rattus norvegicus</i> dihydroorotate dehydrogenase
SBDD	Structure-based drug design
<i>Sh</i>28GST	<i>Schistosoma haematobium</i> glutathione (S)-transferase
<i>Sh</i>DHODH	<i>Schistosoma haematobium</i> dihydroorotate dehydrogenase
<i>Sj</i>DHODH	<i>Schistosoma japonicum</i> dihydroorotate dehydrogenase
<i>Sm</i>DHODH	<i>Schistosoma mansoni</i> dihydroorotate dehydrogenase
<i>Sm</i>DHODHΔloop	<i>Schistosoma mansoni</i> dihydroorotate dehydrogenase Δ loop
SPR	Surface plasmon resonance
TDD	Target-based drug discovery
ULP1	Ubiquitin-like protein 1
WHO	World Health Organization
ΔTm	Thermo shift

Summary

Abstract	i
Resumo	ii
List of Figures	iii
List of Tables	vi
List of Equations	vii
List of Abbreviations	viii
1. INTRODUCTION	12
1.1. Target-based drug discovery	12
1.2. Fragment-based screening.....	13
1.3. Neglected tropical diseases.....	14
1.4. Schistosomiasis	14
1.4.1. History.....	14
1.4.2. Epidemiology	15
1.4.3. Infection and transmission.....	16
1.4.4. Symptoms, diagnosis, and treatment.....	18
1.5. Dihydroorotate dehydrogenase (DHODH)	20
1.5.1. DHODH as a target for schistosomiasis	23
2. OBJECTIVES	23
3. MATERIALS AND METHODS	24
3.1. Protein expression and purification	24
3.2. Enzymatic inhibition assays.....	25
3.3. Compounds library.....	26
3.4. Differential Scanning Fluorimetry (ThermoFMN)	30
3.5. Thermophoresis (MST).....	30
3.6. X-ray crystallography	31
4. RESULTS AND DISCUSSION	31
4.1. Expression, purification, and quantification for <i>Sm</i> DHODH.....	31
4.2. Enzymatic inhibition assays.....	32
4.3. Differential Scanning Fluorimetry (ThermoFMN)	34
4.4. Thermophoresis	38
4.5. Structural analysis.....	41
4.5.1. Overall structure	41
4.5.2. Catalytic loop	43
4.5.3. Protuberant domain	45

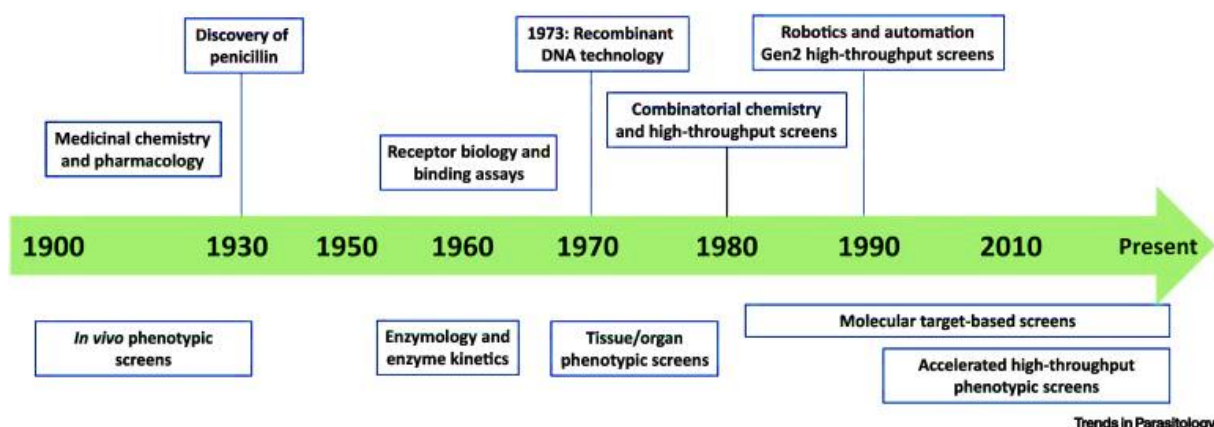
4.5.4. Inhibitor binding-site	49
5. CONCLUSION	53
6. REFERENCES	53
APPENDICES	59

1. INTRODUCTION

1.1. Target-based drug discovery

Embracing different and complex stages, the drug development process comprises from basic research, pre-clinical and clinical studies, until the laborious step of obtaining the regulatory approval of a new drug for sale and marketing (1). This process is long and expensive for the pharmaceutical companies, and involves analysis of safety, efficacy, and its therapeutic benefit to patients - mainly compared with the drugs already available on the market. In 2019, the pharmaceutical industry's research and development (R&D) spending was estimated in \$ 186 billion, and, by 2026, expenditures are expected to reach \$ 230 billion (2). For a new medicine, drug development process takes at least ten years, with an average cost of \$ 2.6 billion (3).

The very first step for identification and development of potential clinical candidates is called drug discovery (DD) (4). DD is divided in two main approaches: target-based (TDD) and phenotypic-based (PDD) (5). The latter was the basis and dominant strategy adopted in the industry until the 1980s (**Figure 1**) and consists of the identification of compounds with the ability to alter a desirable organism or cell's phenotype. By using both *in vitro* and *in vivo* models, PDD still plays an important role in identifying lead compounds and first-in-class drugs, in particular for those that can act through either unknown targets or novel mechanism of actions for known targets



(6).

Figure 1: Phenotypic and target-based approaches timeline (extracted from Aulner, 2019 (7))

However, mainly due to the advance of genetics and recombinant technology (8), and the intrinsic challenges in phenotypic drug discovery, the use of TDD has increased in the last 30 years (6). TDD is based on knowledge of a drug's molecular

mechanism from a much earlier stage and is generally less costly, simpler, and faster (9), despite the drawbacks, like a possible difference in modulation by molecules between *in vitro* and *in vivo* assays (6). TDD explores the direct or indirect involvement of a specific target (genetic or mechanistic – enzymes, receptors etc.) on a disease of interest (target validation) and weighs the drug's ability to induce and/or modulate it on a determined way (10).

Among several number of strategies for TDD applied by academic research groups and the industry over the past 15 years, the fragment-based lead discovery technique (FBLD) has been played a pivotal technology for target discovery and already contributed to the discovery of approved drugs (11).

1.2. Fragment-based screening

The fragment-based screening has been one of the first choices as strategy for analogue-based and structure-based drug design (SBDD), as well as, high-throughput-screening (HTS) and discovering of small molecules (12). FBLD consists basically in the screening of low molecular weight molecules libraries combined with biophysical, structural, and enzymatic assays to develop lead compounds.

The FBLD is sustained by three key elements: i) small number of low molecular weight compounds can cover large areas of chemical space (13); ii) unfavorable interactions increase with the molecules' complexity and weight (12); iii) fragments often bind with better ligand efficiency (LE) than traditional molecules ($LE = -\Delta G/N_{HA}$, where N_{HA} is the number of heavy atoms) (14). In order to produce drug leads with higher affinity, results obtained by using fragments can be combined by linking, merging or growing them (12).

For FBLD several biophysical methods are used to discover low affinity fragments as: surface plasmon resonance (SPR), mass spectrometry (MS), nuclear magnetic resonance (NMR), DNA encoded library (DEL), micro scale thermophoresis (MST), etc. However, due to the low affinities of the initial fragments, these detection methods can infer a variety of artifacts, false negatives, and false positives. To overcome these challenges, X-ray crystallography techniques have more recently been exploited, once that it can provide structural information that enables efficient and rapid assessment of hits with respect to synthetic tractability for SBDD (15). Fragment screening was then selected as the method of choice for this project.

1.3. Neglected tropical diseases.

Although the TDD approach has been extensively used, with a high rate of first-in-class drugs developed by this methodology being approved (16), there are still very few validated drug targets for infectious diseases, in particular, neglected tropical diseases (NTDs), for which the majority of approved drugs have their mechanism of action still poorly understood (17).

Coined in 2003, the term neglected tropical disease (NTD) refers to diseases that share social-geographical features - poverty and burdened entrenched in tropical and subtropical regions (9). Afflicting over a billion people, and with a high rate of mortality and disability, the NTDs impose severe social and economic consequences to developing countries. Currently, the World Health Organization (WHO) recognizes 20 NTDs, including schistosomiasis, dengue, Chagas disease, and leishmaniasis. Despite the recent contribution of pharmaceutical industries, philanthropic organizations, and a massive effort from the academic sector, there is still a lack of adequate treatment for many NTDs, with the main fraction of the registered drugs displaying low efficacy, high toxicity, and high cost (10-12). In the 21st century, the NTDs are still causing numerous cases of death and human suffering mainly in Africa and South America, remaining a serious obstacle to socioeconomic development (18).

In this scenario, caused by trematode worms of the genus *Schistosoma* and responsible for approximately 280,000 deaths annually and 207 million of people infected (13), the schistosomiasis is considered one of the most prevalent NTDs, being the second most important parasitic infection in human after malaria (14).

1.4. Schistosomiasis

1.4.1. History

Schistosomiasis is an old disease. Paleo parasitologists reported the first evidence of parasite eggs in a 6200-year-old grave located at a prehistoric town in Syria. According to the literature, the parasites may have been spread by the

introduction of crop irrigation in ancient Mesopotamia, region that covers parts of modern-day Iran, Iraq, Syria, Kuwait, and Turkey (15). During the Middle Age, individuals infected with *Schistosoma* species were found in Europe, evidencing the parasite migration by persons carrying, but without indication that the life cycle was established in the continent (16). In other countries, as in South America, the schistosomiasis was probably introduced from the slave traffic from Africa (17). The most recent studies indicate six known species responsible for the disease: *S. mansoni*, *S. haematobium*, *S. japonicum*, *S. guineensis*, *S. intercalatum* and *S. mekongi*, being the first three the most common disease-causing (18).

Although being an old and well-known disease, and despite the danger of the disease in spreading and causing more health and economic damage to society (19), the therapeutic drug of choice for schistosomiasis has for decades relied on praziquantel (20). Praziquantel's mechanism of action is not fully understood, and its use displays considerable drawbacks, as the lack of efficiency against schistosomula and juvenile worms (21), poor pharmacokinetics (22) and an unpalatable taste (23), as well evidence of parasite resistance (24-26). The development of an alternative treatment for schistosomiasis is unquestionably urgent.

1.4.2. Epidemiology

Considered the second most important parasitic infection in terms of disability, the schistosomiasis is one of the most prevalent neglected tropical diseases (19). It is caused by *Schistosoma* trematode worms (blood flukes), with snails as the intermediate hosts. More than 700 million people are at risk, and approximately 207 million people are currently infected worldwide, with an estimated number of 280,000 deaths per year (20). Transmission cases were reported in 78 countries (**Figure 2**) with 52 out of these considered endemic regions (21). This disease is prevalent in rural and poor areas that lack access to sanitation and safe drinking water (22).

In Brazil, schistosomiasis is present in 19 states, mainly in Northeast and Southeast regions, affecting about 1.5 million people (23). The physical and, mainly, the cognitive consequences of schistosomiasis directly implicate on the morbidity, being responsible for an annual loss of 4.5 million disability-adjusted life years (DALYs) (24) worldwide. In Brazil, the consequences over the economy are the same once

schistosomiasis directly impacts the productivity. For example, it was estimated that the total cost of schistosomiasis in the country was US\$ 41.7 million in 2015 (25).

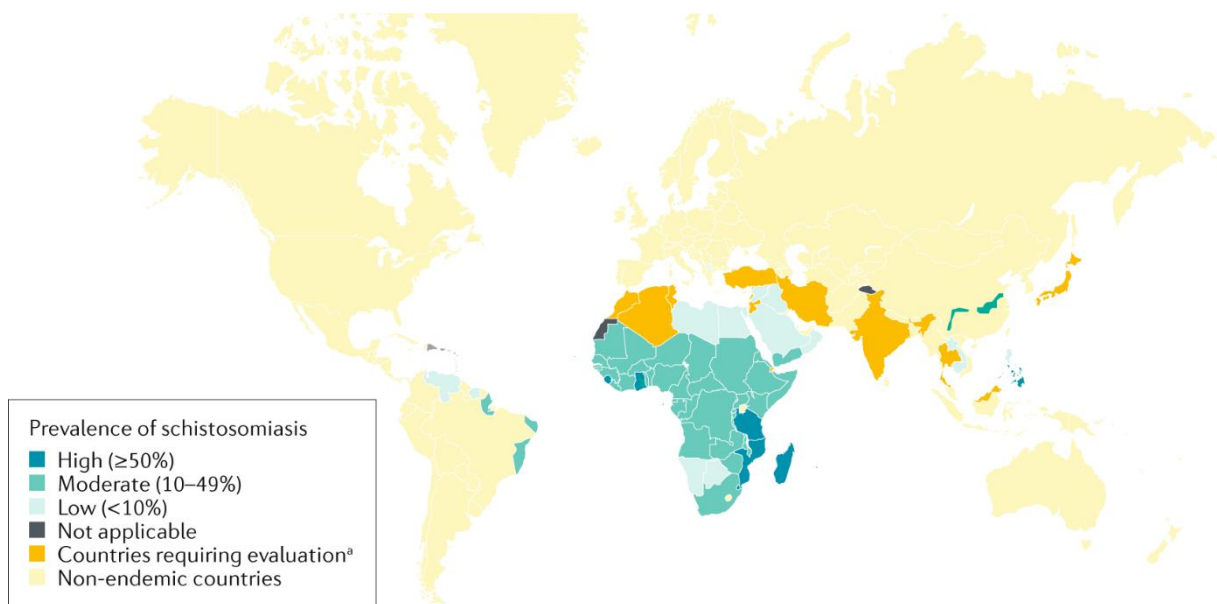


Figure 2: Distribution of schistosomiasis worldwide (Adapted from Map: Distribution of schistosomiasis, worldwide, 2012, WHO, © 2012. Extracted from McManus *et. al*, 2018 (26)).

1.4.3. Infection and transmission

Six known species are responsible for schistosomiasis: *S. mansoni*, *S. haematobium*, *S. japonicum*, *S. guineensis*, *S. intercalatum* and *S. mekongi*, being the first three the most common disease-causing, and only *S. mansoni* found in Brazil (18).

Schistosoma spp. eggs are eliminated by infected humans in urine or feces, starting the cycle of transmission (**Figure 3**). The eggs hatch, releasing the miracidium (ciliated larval form), which swim and penetrate the intermediate host (specifically, in Brazil, the snail of the genus *Biomphalaria*). In the snail occurs the generation of sporocysts and the asexual reproduction generating the cercariae. The cercariae are released and penetrate the human's mucous membranes and/or skin, losing their forked tail and becoming schistosomulae. Once inside the human body, the schistosomulae migrate to the lungs and the heart through venous circulation, finally reaching the liver and developing into sexed forms. Matured adult worms (male and female) exit the liver via the portal vein system, copulate, and settle in the mesenteric venules. Females release the eggs in the small venules of the perivesical and portal systems. The eggs are moved through the lumen of the intestine (*S. mansoni*, *S. mekongi*, *S. japonicum*, and *S. intercalatum/guineensis*) or the ureters and bladder (*S. haematobium*), and are eliminated, restarting the cycle (27, 28).

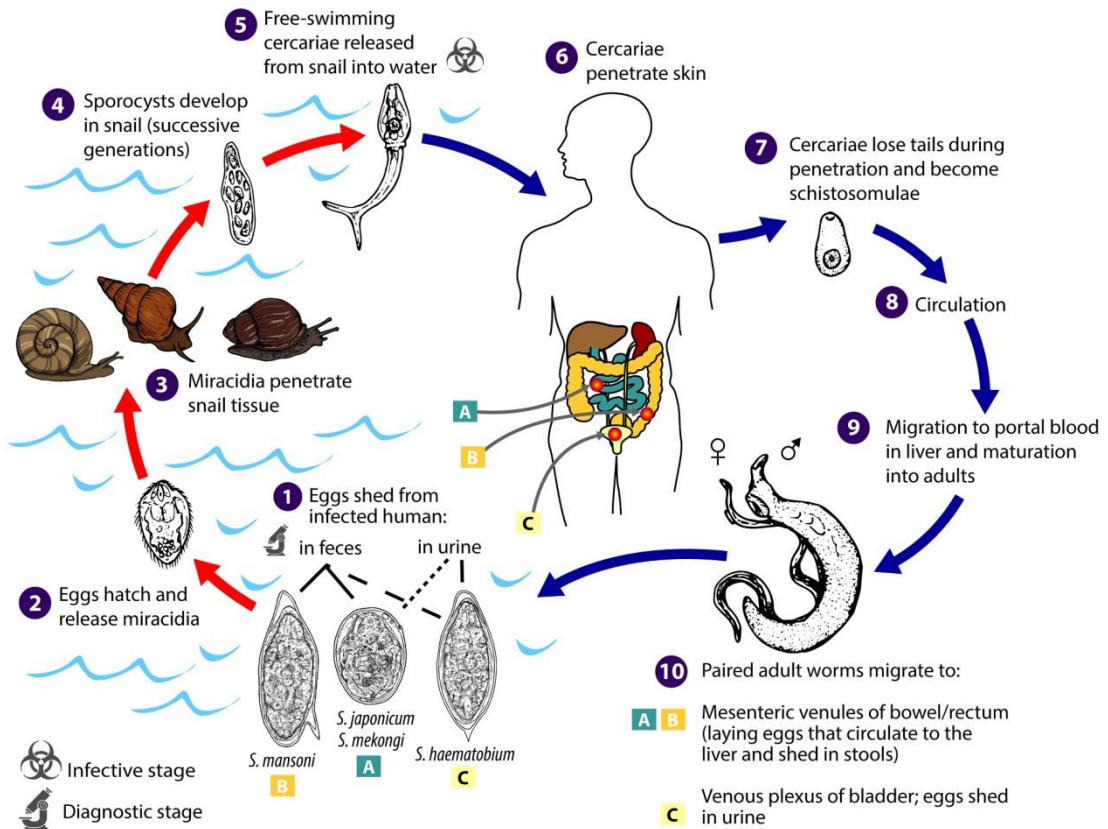


Figure 3: *Schistosoma* spp. life cycle scheme. (Extracted from Centers for Disease Control and Prevention (27)).

A remarkable feature for the *Schistosoma* spp. is the worm pair, where the male adult parasites are tuberculate and robust, measuring approximately 10 mm in width and 6-12 mm in length (**Figure 4**). The females have a slender and cylindrical body, longer than males (7-17 mm in length) (27).

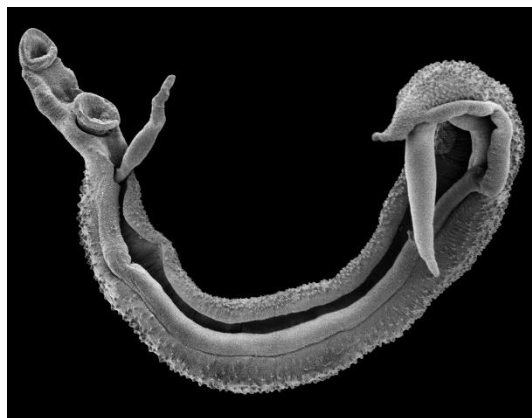


Figure 4: Schistosome worm pair. (Extracted from the Trustees of the Natural History Museum).

1.4.4. Symptoms, diagnosis, and treatment

The symptoms inflicted on the human host and consequences entailed by these diseases are highly relevant and must be not neglected. Symptoms may include from early manifestations, symptoms of acute phase (29), to variable clinical conditions of the advanced and chronic disease. Due to the parasitic and/or eggs presence outside the hepatic portal system, the schistosomiasis can evolve to the ectopic (30), neurological (31), vasculopulmonary (32) and renal (33) forms of the disease.

When people are first infected, most do not develop symptoms. Within a few days after infection, individuals may present an itchy skin or a rash that resemble insect bites. About one to two months later, nonspecific symptoms appear, such as fever, myalgia, diarrhea, non-productive cough, fatigue, and right upper quadrant pain (23, 27).

The symptoms of schistosomiasis are mainly caused by the immune system reaction to the eggs. Eggs that are not eliminated may lodge in the intestine, bladder, or liver, causing inflammation and, in chronic cases, fibrosis (27, 28).

If not treated, schistosomiasis can persist for years, becoming chronic. In this stage, the disease may present several different manifestations. Signs and symptoms include abdominal pain, epigastralgia, enlarged liver, bloody stools and urine. In the most severe forms, eggs lodge in the brain or spinal cord, causing paralysis, seizures, or inflammation of the spinal cord (23, 27).

The most common technique used for diagnosing schistosomiasis is the Kato-Katz method, which consists of identifying and counting the parasite's eggs in the urine or feces. Moreover, a serologic test can be performed to confirm the infection (21, 23, 27).

Praziquantel is the drug of choice for the treatment of schistosomiasis. It displays a broad-spectrum anthelmintic activity, good efficacy and safety, with low cost, used on the treatment of all species of *Schistosoma*, as well some species of trematodes and cestodes (34). However, there are several drawbacks in adopting this therapy for the last four decades. First, although debatable, evidence of parasite resistance have been reported (35-37). In addition, poor pharmacokinetic properties of the oral doses (38), lack of efficiency against juvenile worms and schistosomula (39),

and unpalatable taste (40) affect the patient adherence and increase the risk of reinfection.

Although praziquantel have been used as the preventive chemotherapy via mass drug administration (MDA), its mechanism of action remains not fully understood. The main hypothesis lay on that the schistosome worms calcium ion channels are the target, causing a rapid Ca^{2+} influx and severe spasms and paralysis of the parasite (41-43). Studies have demonstrated that praziquantel can interact with some proteins, as the transient receptor potential channel *SmTRPM_{PZQ}* (44), the calcium binding protein *SmTAL1* (45), and the voltage-gated calcium channel *SmCav1B* (46).

Other perspective to prevent the disease is the vaccine. Currently, no schistosomiasis vaccines are available (26). The main problem is the immunological IgE profile response observed for the schistosome infection. That is also observed for the schistosomiasis vaccine, that stimulating IgE production can also lead to anaphylaxis. The monovalent recombinant protein *S. haematobium* glutathione (S)-transferase (Sh28GST) is the most promising alternative and has been tested in a clinical phase III trial (47). There are other few initiatives for vaccine development in different stages of clinical trials (48-51). Another example is the Sm14/GLA-SE schistosomiasis vaccine, which has achieved the clinical trials phase IIa, showing excellent results regarding tolerance and safety to prevent *S. mansoni* infections (52).

Due to the widespread morbidity and mortality of schistosomiasis, and the lack of alternative treatments and prevention, the present scenario highlights the urgent and unquestionable development of alternative therapeutic strategies against schistosomiasis.

Several approaches have been adopted to control it, from improvement of sanitation and provision of piped water as well as the preventative chemotherapy via mass drug administration (MDA) (53). Some academic and philanthropic initiatives around the world are trying to explore different strategies to overcome this one-drug dependency (54). These projects include drug repurposing, the use of organometallics, natural products, phenotypic and structure-based approaches, among others (55). From the SBDD perspective, there are relatively few validated targets for schistosomiasis. It is our interest to explore target-based approaches to combat this prevalent NTD. Specifically, we intent to evaluate the potential of the enzyme dihydroorotate dehydrogenase (DHODH) as therapeutic target.

1.5. Dihydroorotate dehydrogenase (DHODH)

Dihydroorotate dehydrogenase (DHODH) is a flavoenzyme (EC 1.3.3.1; EC 1.3.99.11) that catalyzes the stereospecific oxidation of (*S*)-dihydroorotate (DHO) to orotate during the fourth and only redox step of the *de novo* pyrimidine nucleotide biosynthetic pathway (**Figure 5**).

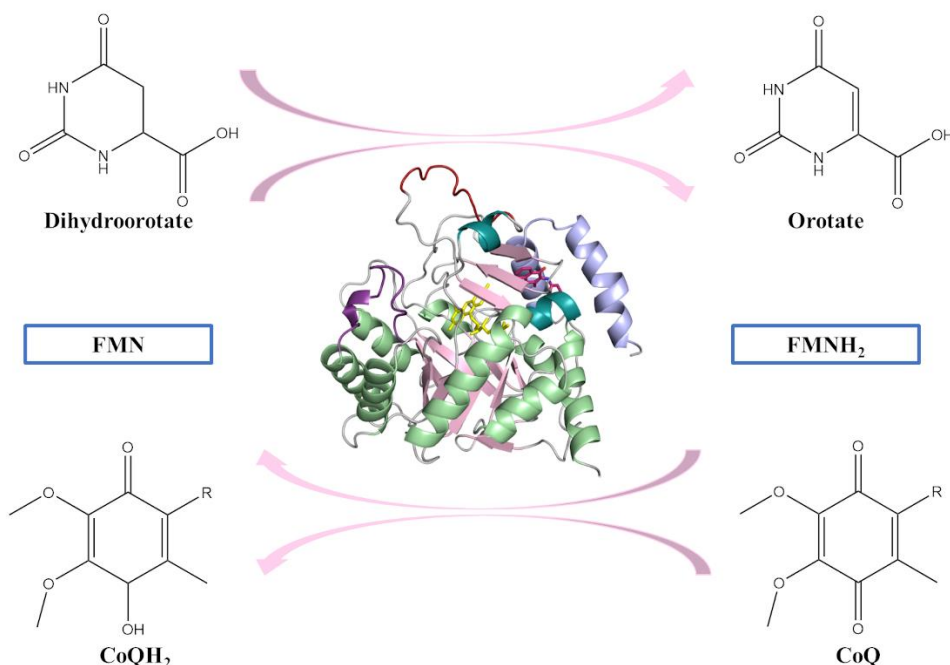


Figure 5: Ping-pong enzymatic reaction catalyzed by class 2 dihydroorotate dehydrogenases (DHODHs). In the first half, the dihydroorotate (DHO) is oxidized to orotate, accompanied by the reduction of the prosthetic group flavin mononucleotide FMN to FMNH₂. In the second part, FMN is reoxidized (FMNH₂ is converted to FMN) by the final electron acceptor - ubiquinone (Extracted from Mori, RM. *et al*, 2020. (56)).

DHODH catalysis DHO oxidation to orotate, accompanied by the reduction of the prosthetic group flavin mononucleotide FMN to FMNH₂. In the next half-reaction, FMN is reoxidized (FMNH₂ is converted to FMN), for new cycles of catalysis, by a second substrate that acts as an electron acceptor (**Figure 5**) (57). According to their cell location and preferences for electron acceptors, DHODHs are divided into two major classes. Class 1 enzymes are found in the cytosol and utilize soluble substances as their final electron acceptor, whereas enzymes belonging to class 2 are associated with cytosolic or mitochondrial membranes and use respiratory quinones to reoxidize the flavin group (56). DHODHs have been considered important drug targets for cancer, autoimmune and parasitic diseases, as well viral, fungal, and bacterial infections (58-64). DHODH catalyzes the rate-limiting step in the *de novo* pyrimidine

nucleotide biosynthetic pathway. Therefore, inhibition of DHODH lowers the intracellular pools of cytosine, uracil, and thymine nucleotides (57). Moreover, the use of respiratory quinones as their physiological electron acceptor links the mitochondrial respiratory chain to the pyrimidine biosynthetic pathway (65, 66). Finally, the orotate (product of the catalysis) was reported to be involved in gene transcription regulation (67).

The *Schistosoma mansoni* dihydroorotate dehydrogenase (*Sm*DHODH) belongs to class 2 DHODHs. Class 2 DHODHs are monomers that commonly present two canonical domains: an N-terminal helical domain folds into two α -helices linked by a short loop, and a C-terminal domain consisting of an α/β barrel (57). In all class 2 enzymes, the N-terminal domain forms a tunnel that is known as the target for class 2 inhibitors, and where is hypothesized to be the quinone binding site. Although the conserved secondary structures elements among the class 2 DHODHs (68), the variability observed within the helical N-terminal domain (α A and α B) (**Figure 6**) has been studied to design selective inhibitors among members of class 2 DHODHs (57).

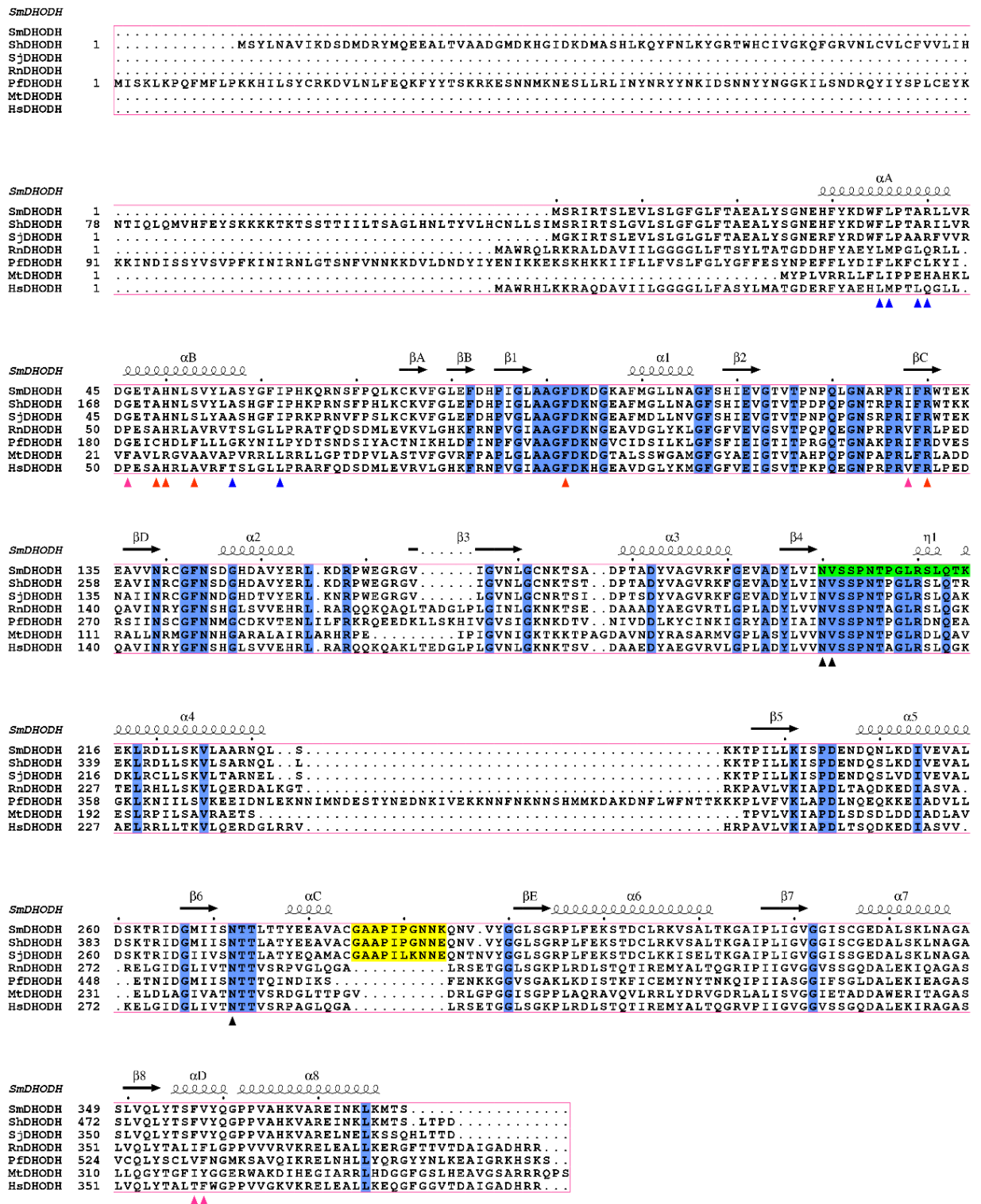


Figure 6: Sequence alignment of selected class 2 DHODHs: *SmDHODH* (*Schistosoma mansoni* DHODH; UniProt entry: **G4VFD7**), *ShDHODH* (*Schistosoma haematobium* DHODH; UniProt entry: **A0A094ZN75**), *SJDHODH* (*Schistosoma japonicum* DHODH; UniProt entry: **Q5DD85**), *RnDHODH* (*Rattus norvegicus* DHODH; UniProt entry: **Q63707**), *PfDHODH* (*Plasmodium falciparum* DHODH; UniProt entry: **Q08210**), *MtDHODH* (*Mycobacterium tuberculosis* DHODH; UniProt entry: **P9WHL1**) and *HsDHODH* (Human DHODH; UniProt entry: **Q02127**). Residues that interact with O230 are indicated by red arrows, and those that interact with the glycerol by black arrows. Residues that vary between *HsDHODH* and *SmDHODH* along the binding channel are indicated by blue arrows. Residues that

interact with the 0230 and vary along the pocket are indicated by pink arrows. The protuberant region (Gly²⁸⁵ – Lys²⁹⁴) is highlighted yellow for the *Schistosoma* spp., and the catalytic loop (Asn²⁰⁰ – Lys²¹⁵) is in green. The alignment was performed using MULTALIN (69) and graphically displayed using ESPript 3.0 (70). (Extracted from Mori, R.M. *et al.*, 2020 (56)).

1.5.1. DHODH as a target for schistosomiasis

As described, DHODHs lay at the center of critical biochemical pathways and therefore can be an excellent drug target against schistosomiasis. With this, the DHODH inhibition has gained medical relevance for academia and industry (57). For example, the leflunomide and its metabolite teriflunomide has been shown to inhibit human DHODH (*HsDHODH*) (71), as well as, the brequinar sodium (72), that it has been evaluated as anti-cancer and immuno-suppressive agent. Moreover, the *Plasmodium falciparum* DHODH (*PfDHODH*) has been studied as target for malaria (73).

Previously, our team characterized the *SmDHODH* by homology modeling, molecular dynamics, and kinetic studies (68). These results indicated differences in conformational changes comparing the *SmDHODH* and its human homolog enzyme (*HsDHODH*), as well as amino acid substitutions that can grant inhibitor selectivity. Subsequent studies allowed us to identify atovaquone - a hydroxy-1,4-naphthoquinone used in the treatment of malaria, as a selective inhibitor in the nanomolar range against the *SmDHODH* (68). Those results prompted us the idea of exploiting the parasitic enzyme as search for drug leads against schistosomiasis.

2. OBJECTIVES

The aim of the present work was to identify ligands for *Schistosoma mansoni* dihydroorotate dehydrogenase by a target-based drug discovery approach focused on fragment screening. For such studies, our proposal involved the screening of fragments and the structural, biochemical, and biophysical characterization of the enzyme in presence of identified ligands. Thus, the following steps were accomplished:

- Heterologous expression and purification of *SmDHODH* using *E. coli* as the expression system;

- Ligand screening and characterization by differential scanning fluorimetry, enzymatic assays and thermophoresis;
- Structural studies by X-ray crystallography.

3. MATERIALS AND METHODS

3.1. Protein expression and purification

The gene was cloned according to Nonato *et al.*, 2019 (68), where the gene sequence coding for *SmDHODH* (GenBank ID: XM_002578964) was amplified by PCR using primers that were designed to obtain a truncated version of the enzyme (Leu23 – Ser379) (GenBank ID: CCD78646) (68) and cloned into pET-28-SUMO-*SmDHODH*. A single colony of *E. coli* BL21-CodonPlus (DE3)-RIL was transformed with the plasmid and grown overnight in 10 mL of medium (1 g/L KH_2PO_4 , 2 g/L Na_2HPO_4 , 8 g/L NaCl, 15 g/L yeast extract and 20 g/L bacto-tryptone) containing 34 $\mu\text{g}/\text{mL}$ chloramphenicol and 30 $\mu\text{g}/\text{mL}$ kanamycin at 180 rpm and 37 °C and used to inoculate 1 L of fresh medium. When the O.D 600nm reached 0.5, isopropylthio- β -galactoside (IPTG) was added to 100 μM final concentration and the temperature was reduced to 18 °C. After 24 hours the cells were isolated by centrifugation at 10,000 g for 8 minutes and kept at -20°C.

Cell pellets corresponding to 500 mL of culture were resuspended in 20 mL of lysis buffer (1 mM phenylmethanesulfonylfluoride (PMSF), 50 mM Tris-HCl pH 7.5, 600 mM NaCl, 0.33% Thesit (Sigma), 10% glycerol and EDTA-free SigmaFAST™ (Sigma) protease inhibitor cocktail). The cells were lysed using 15 cycles of 30s sonication with 30s intervals on ice with an output power of 10W. The lysate was then maintained on ice for 30 minutes on a rocking shaker and centrifuged at 16,100g for 30 minutes at 4 °C.

The soluble fraction was loaded into a 1 mL HisTrap™ HP column connected to an ÄKTA-Purifier system (GE Life Sciences) previously equilibrated with buffer A (50 mM Tris-HCl pH 7.5, 600 mM NaCl, 0.05% Thesit, 10% glycerol). An chromatographic run was carried out at 1.0 mL/min. The wash steps to eliminate contaminants consisted of passing through at least 5 column volumes of buffer A containing 25 mM imidazole

followed by 5 column volumes of buffer A containing 50 mM imidazole. 6xHis-SUMO-DHODH was eluted with buffer A containing 500 mM imidazole. The eluted samples were concentrated to 500 μ L using a 10 kDa cutoff Amicon Centrifugal and desalted by completing the volume to 10 mL with buffer A containing 0 mM imidazole (4x).

Homemade 6xHis-ubiquitin-like protein 1 (ULP1) protease was incubated with the desalted protein, during 16 hours at 4 °C. The sample was once again loaded into a 1 mL HisTrap™ HP column connected to an ÄKTA-Purifier system (GE Life Sciences) pre-equilibrated in buffer A. Tag-free DHODH was collected in the flow through. The 6xHis-SUMO tag and 6xHis-ULP1 were eluted from the column with buffer A containing 500 mM imidazole.

The target protein was further purified by size exclusion chromatography performed on an Äkta Purifier system (GE Healthcare Life Science®, Uppsala, Sweden) at 6 °C. SmDHODH, previously dialyzed against 600 mM NaCl, 50 mM Tris-HCl pH 7.5, 10% glycerol, 0.05% Thesit was concentrated, and applied to a Superdex 200 (10/300) GL column (GE Healthcare Life Science®, Uppsala, Sweden) pre-equilibrated with 500 mM NaCl, 50 mM Tris-HCl pH 8.5, and 0.05% Thesit at flow rate of 0.5 mL/min. Protein elution was monitored at 450 nm. Fractions eluted from the size column were pooled and concentrated using a 10 kDa cutoff Amicon Centrifugal (Millipore, Burlington, MA, USA) (56).

3.2. Enzymatic inhibition assays

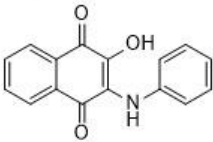
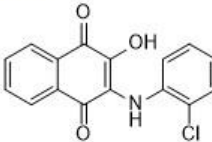
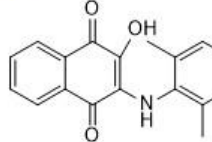
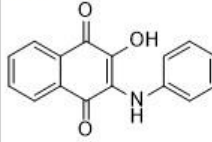
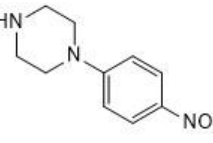
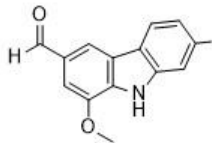
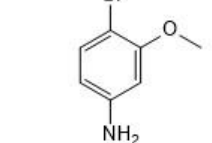
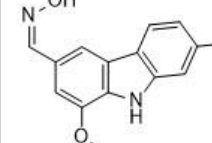
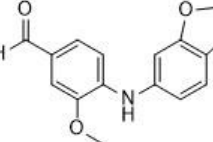
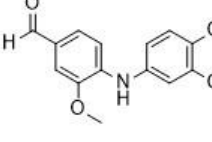
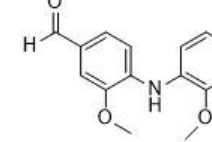
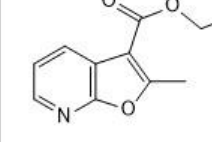
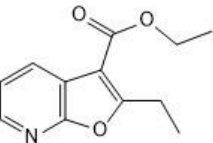
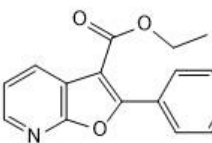
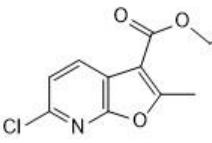
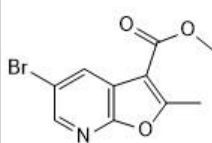
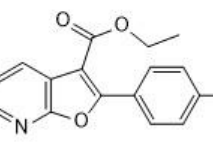
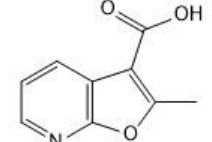
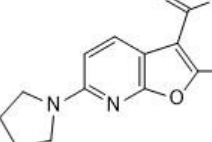
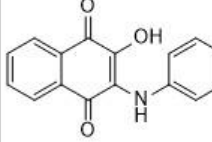
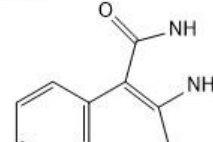
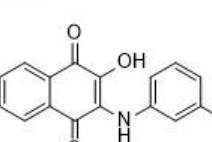
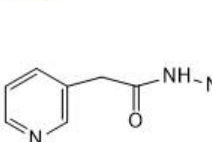
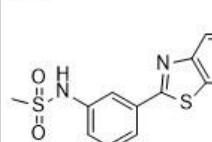
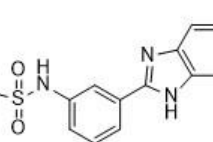
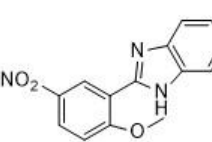
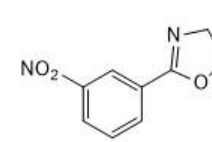
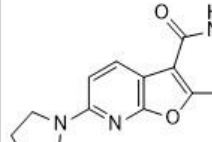
The experiments were performed in a 96-well microplate reader, containing 60 μ M dichlorophenolindophenol (DCIP), 50 mM Tris pH 8.15, 150 mM KCl, 0.1 % Triton X-100, 500 μ M DHO, 100 μ M CoQ₀ and varied inhibitor concentrations. To start the reaction, 5 μ L SmDHODH protein solution was added, to a final concentration of 20 nM. As a negative control, 5 μ L of enzyme was added to 200 μ L buffer, without the presence of the inhibitors. As a positive control, 5 μ L of enzyme was added to 200 μ L buffer, with the presence of a known inhibitor (α -Lapachol). The reaction was monitored each 3s over a period of 60s, in triplicate, for each concentration and each tested compound. All the compounds tested belong to the library described in the topic 3.3. The IC₅₀ was determined through the graph of percent of inhibition versus log of the inhibitor concentration. The dose-response curve was fit according to **Equation 1** using OriginPro 8 software.

$$y = \frac{A1 + (A2 - A1)}{1 + 10^{(\log x_0 - x) * p}}$$

Equation 1: Sigmoidal fitting equation used (dose response). Where A1 corresponds to the minimum inhibition value, A2 corresponds to the maximum inhibition value, p corresponds to the Hill slope and LOGx0 corresponds to the inflexion point that correspond to the inflexion point that correspond to the inhibitor concentration responsible for 50% loss of enzymatic activity.

3.3. Compounds library

A group of 52 compounds was evaluated as *Sm*DHODH inhibitors (**Figure 7**). The compounds tested have a molecular weight's average of 278 Da. The molecules were synthesized and kindly donated by Professor Flávio Emery's group (FCFRP/USP).

0009 	0011 	0012 	0034 
0040 	0052 	0053 	0064 
0066 	0111 	0113 	0209 
0212 	0213 	0215 	0217 
0218 	0219 	0227 	0230 
0295 	0297 	0310 	0320 
0321 	0324 	0326 	0331 

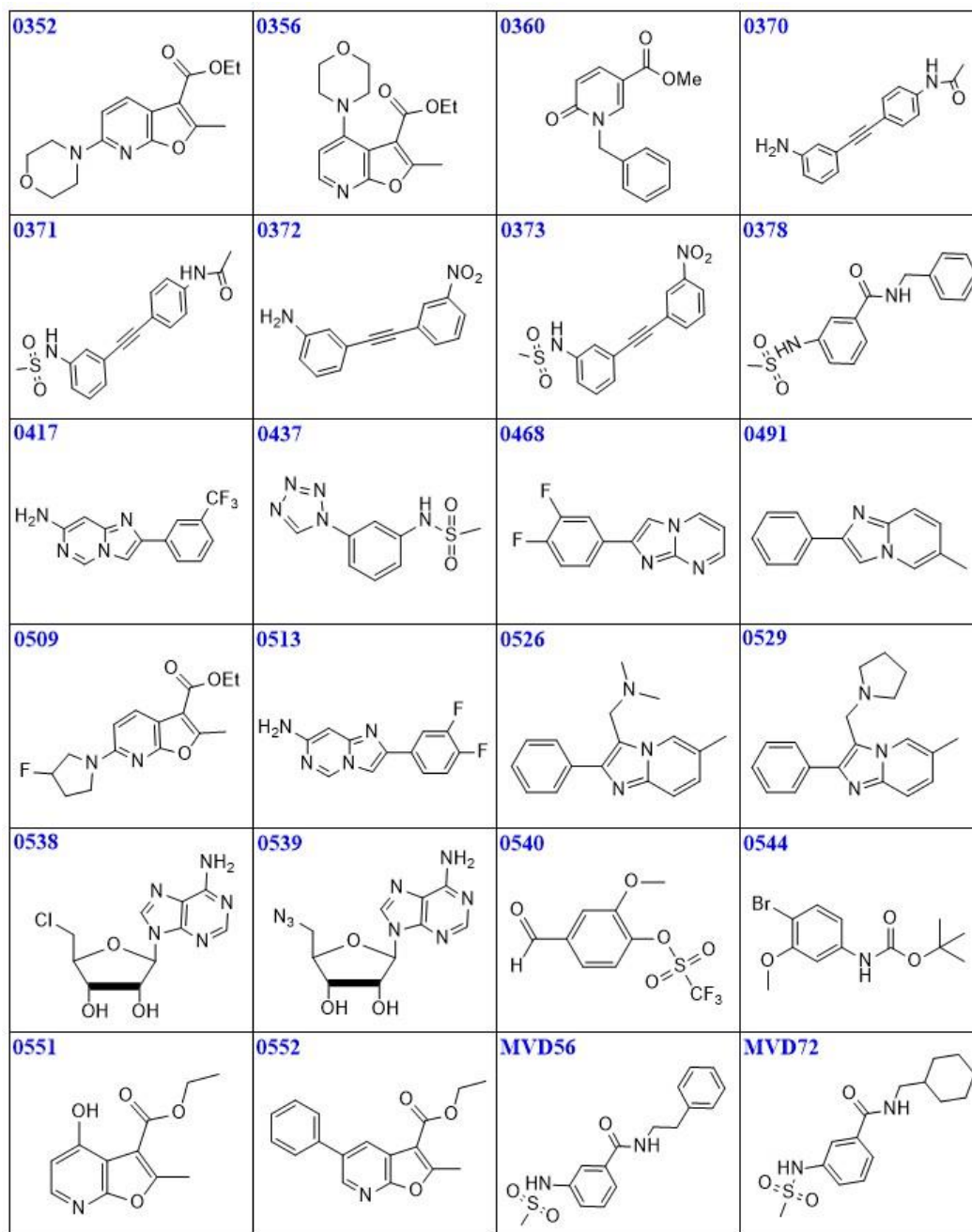


Figure 7: Two-dimensional structure representation of the compounds donated by Professor Flávio Emery's laboratory and tested against SmDHODH by ThermoFMN, enzymatic inhibition and crystallization assays. The IC₅₀ values (μM) were obtained for the compounds 0009; 0011; 0034; 0230; 0297 and 0320.

Additionally, to investigate the role of different fragment scaffolds interacting with the protuberant domain described in the structural analysis, ThermoFMN technique was applied on both *SmDHODH* and *SmDHODH*Δloop constructs. ThermoFMN was used to compare the thermal stability effects to the IC₅₀ against a

library of atovaquone-analogues that was previously tested by our group against the native protein (**Figure 8**) (74).

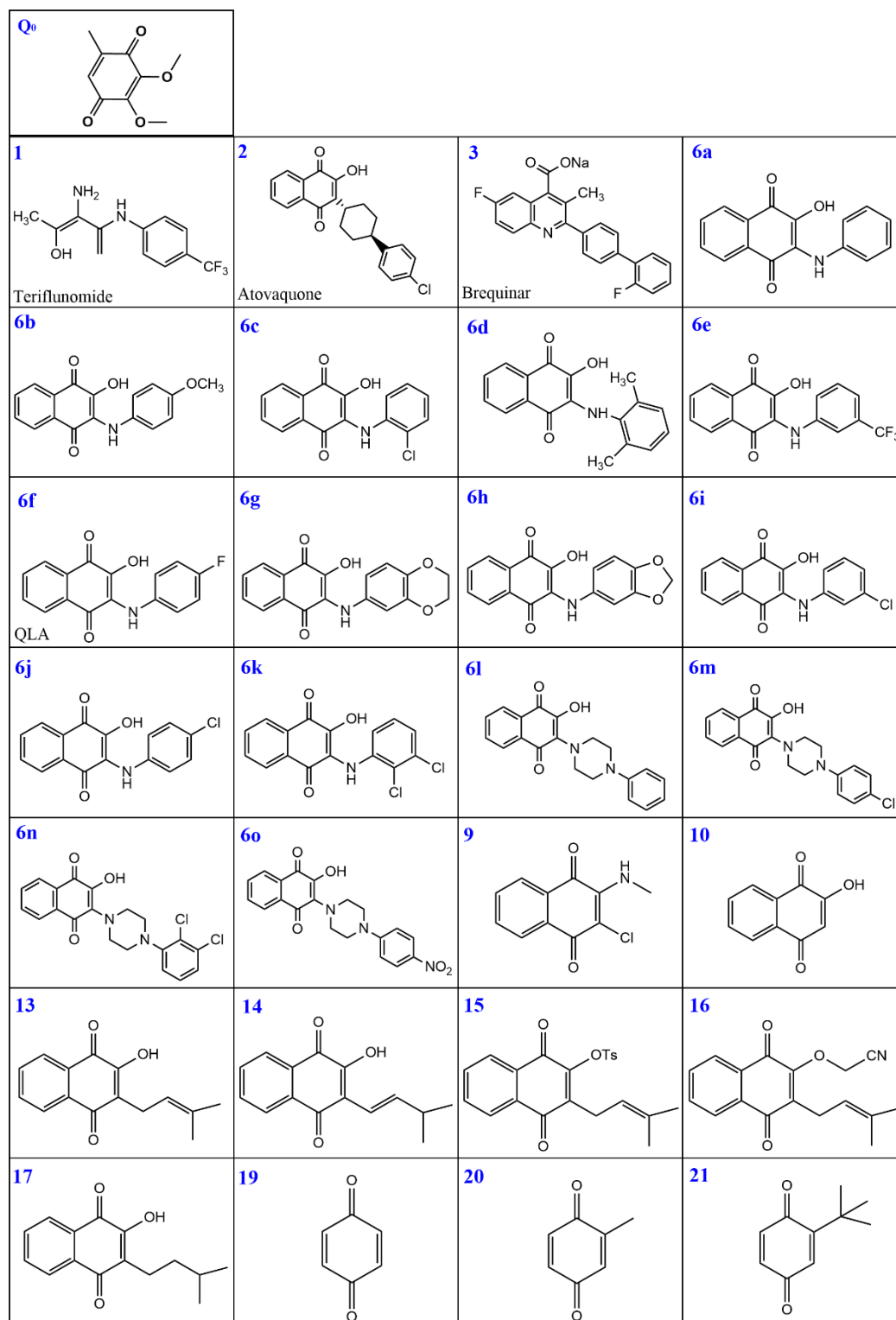


Figure 8: Two-dimensional structure representation of atovaquone-based compound library evaluated as *SmDHODH*-inhibitors (74), and the coenzyme Q₀. Compound 1 is teriflutnomide, 2 is atovaquone and 3 is brequinar. Compounds 6a to 6k are simplified analogs of atovaquone, classified as 0230-like

compounds. Compounds (6l - 6o) were classified as atovaquone-like series. Numbers 9 and 10 are 1,4-naphthoquinones derivatives and from 13 to 17 are lapachol derivatives. Compounds 19, 20 and 21 are benzoquinones. (Extracted from Mori, RM. et al. (56)).

3.4. Differential Scanning Fluorimetry (ThermoFMN)

Differential scanning fluorimetry assays were developed, as described in Mori *et al.*, 2020 (56), in a thermocycler – Mx3005P™ Real-Time PCR system (Agilent Technologies, Santa Clara, CA, USA). The experiments were performed in triplicate in a 96-well PCR plate (Agilent Technologies, Santa Clara, CA, USA), where each well contained 10 μ L enzyme at 10 μ M (5 μ M final concentration), and 10 μ L of different compounds at 500 μ M (final concentration). The fluorescence intensity was monitored using the filter FAM SyBr green I, 492 nm and 516 nm, excitation, and emission, respectively. The temperature varied from 25 to 95 °C (1 °C/min). The curves obtained were used to determine the melting temperature (T_m) (inflexion point) using the software GraphPad Prism 5.03 (www.graphpad.com).

3.5. Thermophoresis (MST)

The MST assays were developed on a NanoTemper Monolith equipment using the NanoTemper RED-MALEIMIDE kit, which fluorescently labels protein cysteine residues. The experiments were performed at the Institute of Physics São Carlos, University of São Paulo. *SmDHODH* was purified and labelled according to the labelling kit protocol. Both labelled protein concentration and labelling degree were calculated from A205, A650, and A280 absorbance using equations in the labelling kit manual. The MO. Control software was used in all experiments. Stock concentrations of selected compounds (0009; 0011; 0230) were prepared in 100% DMSO (5 mM). The dilution set contained 10 μ L of 10 nM labelled *SmDHODH* (diluted in MST buffer) and 10 μ L of the compound stocks (final concentration 2.5 mM). The dilution set was incubated, centrifugated and 10 μ L loaded into standard capillaries. MO Affinity Analysis software was used to analyze the MST traces to calculate the binding check.

3.6. X-ray crystallography

The crystallographic experiments were performed as described in Mori *et al.*, 2020 (56). Crystals of *SmDHODH* recombinant enzyme were obtained in the presence of citric acid and 2-(N-morpholino)ethanesulfonic acid (MES). Crystallization experiments were carried out by the sitting drop vapor diffusion method, using 5 μM *SmDHODH* (concentration calculated based on the extinction coefficient of FMN) at 21 °C. Drops were prepared by mixing 1.0 μL of protein solution and 1.0 μL of reservoir solution containing 1.3–1.5 M citrate pH = 7.0 in 0.1 M MES pH 6.5.

The data set was collected at 100 K on the PROXIMA2 protein crystallography beamline at SOLEIL, France using an EIGER X 9M detector (Dectris, Baden, Switzerland). 1800 frames with an oscillation step of 0.1° were collected using an exposure time of 0.025s per image with a crystal-to-detector distance of 280 mm. X-ray diffraction data were processed and scaled with *XDS* (75) and *AIMLESS* (76). The structure of *SmDHODH* was solved by molecular replacement using the program phaser (77), contained within in Phenix suite (78). The coordinates of a different *SmDHODH* structure at 2.2 Å (PDB: **6UOY**; MORI, RM, ZAPATA, LCC and NONATO, MC; unpublished results) were used as template. The structure was refined with phenix.refine (79), followed by manual map inspection and model building using coot (80). The quality of the model was regularly checked using MOLPROBITY (81). The structural figures were prepared with PYMOL (82).

Coordinates and structure factors have been deposited in the PDB with the accession code **6UY4** (56).

4. RESULTS AND DISCUSSION

4.1. Expression, purification, and quantification for *SmDHODH*

The expression and purification protocols previously established in the laboratory (67) were adapted to improve yield and to speed up the purification protocol. The yield obtained, measured at 280 nm, is reproducible and around 48 mg per liter of culture for *SmDHODH*. SDS-PAGE gels show that the constructs were overexpressed in the soluble fraction and purification was successfully achieved by nickel affinity chromatography.

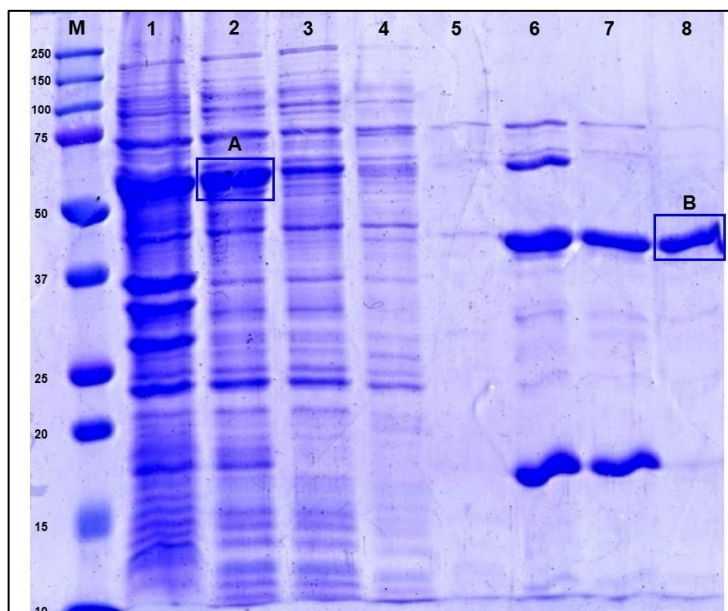


Figure 9: SDS-PAGE analysis of nickel affinity chromatography showing the purification steps. M: molecular weight marker. **A:** SmDHODH + 6xHis-SUMO-tag. **B:** Purified protein. 1: Insoluble fraction; 2: Soluble fraction; 3: Flowthrough; 4: Washing step containing 10 mM imidazole; 5: Washing step containing 25 mM imidazole; 6: Protein elution containing 500 mM imidazole; 7: Protein after cleavage; 8: Protein after second affinity chromatography.

4.2. Enzymatic inhibition assays

Activity measurements were obtained by the indirect assay through monitoring DCIP reduction at 610 nm. The method was chosen once that most part of the compounds absorb close to orotate (product of catalysis) maximum absorption wavelength (300 nm). An initial screening with 52 compounds at single dose concentration (200 μ M) allowed us to select a subset of molecules that inhibit SmDHODH (**Table 1**).

Table 1: Compounds tested in the initial screening at 200 μM against *SmDHODH*. Their respective codes and percent of inhibition.

CODE	% Inhibition	CODE	% Inhibition	CODE	% Inhibition	CODE	% Inhibition
0009	97.1	0213	7.1	0326	-0.4	0491	2.9
0011	99.6	0215	15.8	0331	2.1	0509	0.0
0012	99.6	0217	11.3	0352	0.0	0513	12.5
0034	99.6	0218	8.8	0356	1.7	0526	18.3
0040	0.0	0219	7.1	0360	0.0	0529	0.0
0052	8.3	0227	10.0	0370	7.9	0538	0.0
0053	5.0	0230	98.8	0371	20.0	0539	5.0
0064	3.7	0295	4.2	0372	0.0	0540	13.3
0066	1.3	0297	99.2	0373	7.1	0544	1.7
0111	5.0	0310	0.0	0378	15.8	0551	6.7
0113	11.3	0320	89.6	0417	0.0	0552	19.2
0209	0.0	0321	5.0	0437	4.6	MVD 56	12.5
0212	7.1	0324	16.7	0468	9.2	MVD 72	17.5

Compounds that inhibited *SmDHODH* more than 80% in single concentration assay had their IC_{50} values calculated by non-linear regression fit (**Table 2**).

Table 2: IC_{50} values (μM) obtained for *SmDHODH* against the compounds 0009; 0011; 0034; 0230; 0297 and 0320. *Curve for compound 0012 was not obtained.

CODE	IC_{50} (μM)	CODE	IC_{50} (μM)
0009	2.9 ± 0.4	0230	0.83 ± 0.09
0011	0.05 ± 0.01	0297	0.23 ± 0.02
0034	0.14 ± 0.01	0320	16 ± 4

With exception of the compound 0320, all the potent inhibitors that showed the best IC_{50} values are atovaquone analogs (**Figure 10**), a hydroxy-1,4-naphthoquinone used in the treatment of malaria that was previously identified as a selective *SmDHODH* inhibitor in the nanomolar range (68).

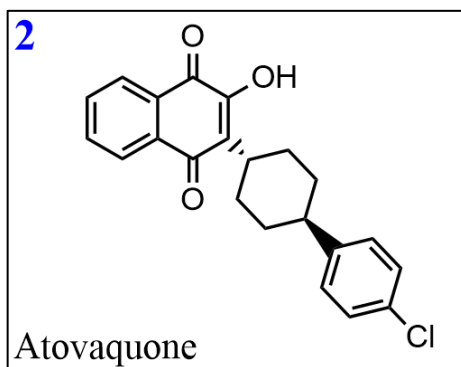


Figure 10: Two-dimensional structure of atovaquone

4.3. Differential Scanning Fluorometry (ThermoFMN)

Validation of hits is a vital component of the fragment-based drug discovery strategy. Therefore, the same 52 compounds were submitted to thermostability assays (**Figure 11**) to estimate protein stability by using differential scanning fluorimetry (DSF) alternative technique called ThermoFMN (83). In DSF, the protein unfolding process is monitored as a function of increasing temperature. However, once detergent (Thesit®) is present in the purification procedure, the traditional methodology is infeasible. Therefore, the ThermoFMN technique was applied. In this technique, DSF is performed in the absence of dye, exploring the prosthetic group FMN from flavoproteins as the fluorescence marker. The unfolding process can then be followed by monitoring differences in fluorescence intensity. The fluorescence intensity is plotted as a function of temperature, and the curve inflexion point allows the determination of the protein melting temperature, T_m .

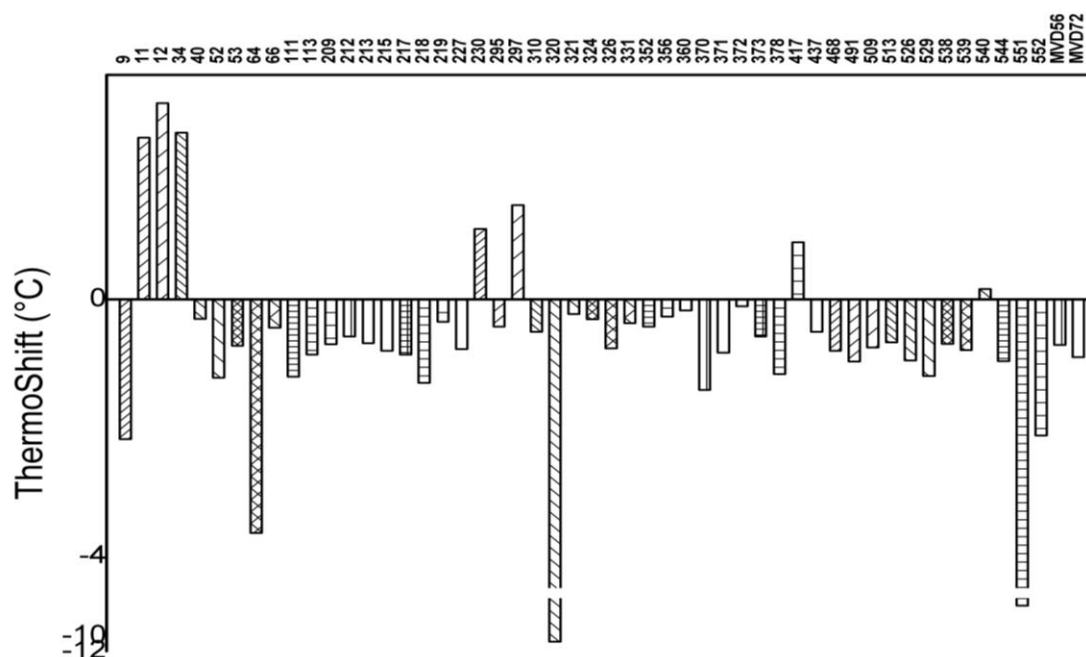


Figure 11: ΔT_m shifts for the tested compounds at 2 mM against *SmDHODH* from reference of 55.07°C.

Although some compounds have presented significant enzymatic inhibition - as described before, it is possible to observe a different thermal shift behavior between the compounds 0011, 0034, 0230 and 0297 compared to the molecules 0009 and 0320. The first four display positive thermal shifts, whereas the latter two large negative thermal shifts. In previous analysis by our group (84) was hypothesized that the different mechanisms of action could influence distinct thermo shifts by inducing the FMN release or by stabilizing the protein, although both molecules inhibit the protein in equivalent magnitude. Molecular dynamics studies have also shown a structural plasticity involving the *SmDHODH* N-terminal α -helical domain (68). Since the studies involving the class 1A DHODHs (85), it was highlighted the complexity of the catalysis control in these enzymes. The same is observed for class 2, and, in the case of the schistosome's DHODH, a protuberant domain also can implicate in this catalytic orchestra (as it will be elucidated in the topic 4.5.3). Therefore, even between fragments with the same scaffold, as the atovaquone analogs 0011/0034/0230/0297 and the 0009 it is reasonable to speculate that they display different binding modes. The fact that, quinone itself, the oxidant agent induces a negative thermo shift, suggests to us that the compounds that induce negative thermo shift are, in fact, binding in a conformation expected for the second and oxidative step to occur. Probably, the compounds with positive thermal shift have a propensity to protect the

protein from thermal denaturation (stabilizing the protein), by stabilizing the active site loop in its closed conformation.

We also tried to correlate the thermo shift results with compound features. Therefore, we clustered the fragments in eight groups (**Figure 12**) according to their chemical features. It was possible to observe that structural patterns, and thus the spatial organization for their interaction with the target dominates the tendency towards the thermo shift profile (positive, negative, or neutral – not significant).

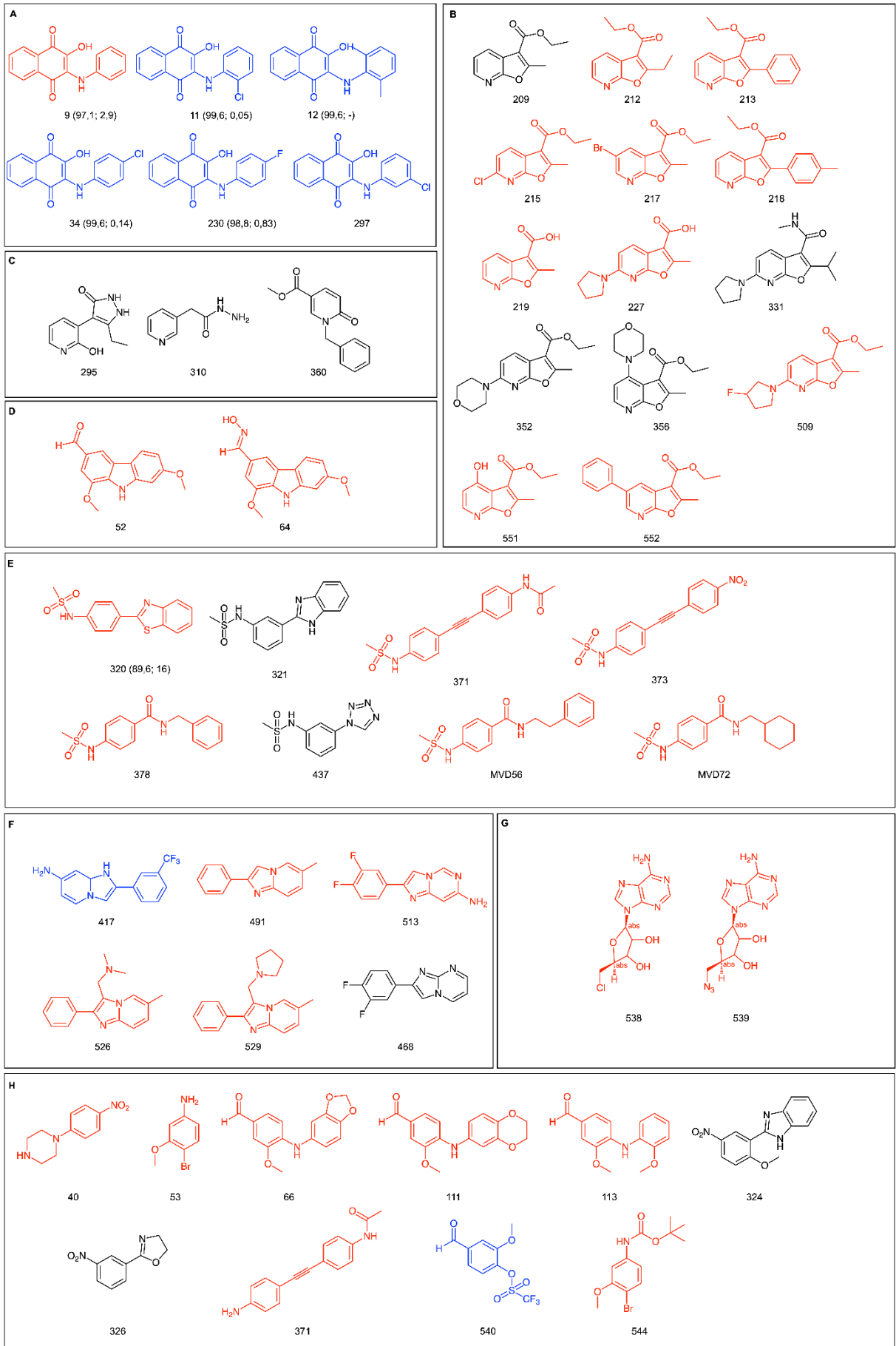


Figure 12: Fragments tested against *SmDHODH*. Fragments with positive thermo shifts are colored in blue, those with negative thermo shifts in red, and the fragments classified as neutral in black (no significant deviation). Structural patterns: A) hydroxynaptoquinones, B) furopyridines; C) pyridines; D) carbazole; E) Sulfonamides; F) imidazopyridines and imidazopyrimidines; G) methanocarb; H) aromatics. For compounds 9, 11, 34, 230, 397 and 320 the percentage of inhibition (IC₅₀ in μM) is presented.

The naphthoquinones (group A) show positive ΔT ms (0011, 0012, 0034, 0230 and 0297), with exception of one fragment that showed a tendency for negative ΔT m (0009). In this specific case, this does not seem to affect the activity, since they had the same inhibition profile, despite the slightly higher IC₅₀ for 0009.

For the furopyridine series (group B), the trend towards negative thermo shift is clear, regardless the substitution pattern on the furan or pyridine side, although the values tending to neutral when the morpholine is introduced in the pyridine ring (0352 and 0356). However, it is not possible to speculate more about this series, which would need a larger data set to evaluate the properties governing the interaction with the enzyme. This same thermoshift profile is observed in the group E. But, in this case, it is possible to verify the importance of the thiazole ring (0320) in the series of compounds containing the sulfonamide function, since in this specific case the negative thermoshift is significant, which evidences the importance of the aromaticity and polarizability (comparing with the 0321). In series with a lower number of specimens, such as the groups C, D and G, the trend according to the structural pattern is also suggested (**Figure 12**). On the other hand, in the groups F and H, the analysis can be even more complex, given the variability of results for the small number of compounds.

In terms of physical-chemical properties, it is also not possible to make a clear correlation between the observed thermo shift pattern and properties related to polarity and electronic distribution, among others. When observing the series of compounds, grouped by thermo shift profile, it is not possible to highlight any physical-chemical properties (cLogP, hydrogen acceptor or donor groups, polar surface area, molecular weight, or structural similarity) that are influencing on the observed experimental result.

4.4. Thermophoresis

As proposed in our project, we planned to use the Micro Scale Thermophoresis (MST) to estimate binding affinity of the identified compounds. The MST experiments were planned to be performed at the multiuser laboratory at Instituto de Física de São

Carlos (<http://www.ifsc.usp.br/emu-mst/>). In our attempts it was possible to successfully label the protein with the cysteine probe during the pretest stage (**Figure 13A**). However, at the binding check step (in the presence of different compounds), we were not able to implement a reproducible protocol (**Figure 13B**) and consequently to proceed to binding affinity determination. The quality of the MST traces in the presence of the compounds (**Figure 13B**) can indicate different problems (86) that could be optimized for future studies. Gradual changes among the capillaries influence directly on the MST traces. Therefore, salt conditions should be avoided (600 mM NaCl) (87). The compounds, due its insolubility in aqueous buffer, are dissolved in DMSO. However, DMSO can reduce protein stability in the capillaries, with this, decrease the DMSO percentage (5% to 2.5%) or change the buffer (for DMF, ethanol, or similar) could also improve the results (86). Finally, to avoid protein aggregation, the detergent Tween-20 was added to the assay buffer, but if it has not kept constant in each capillary problems in MST can be observed (87).

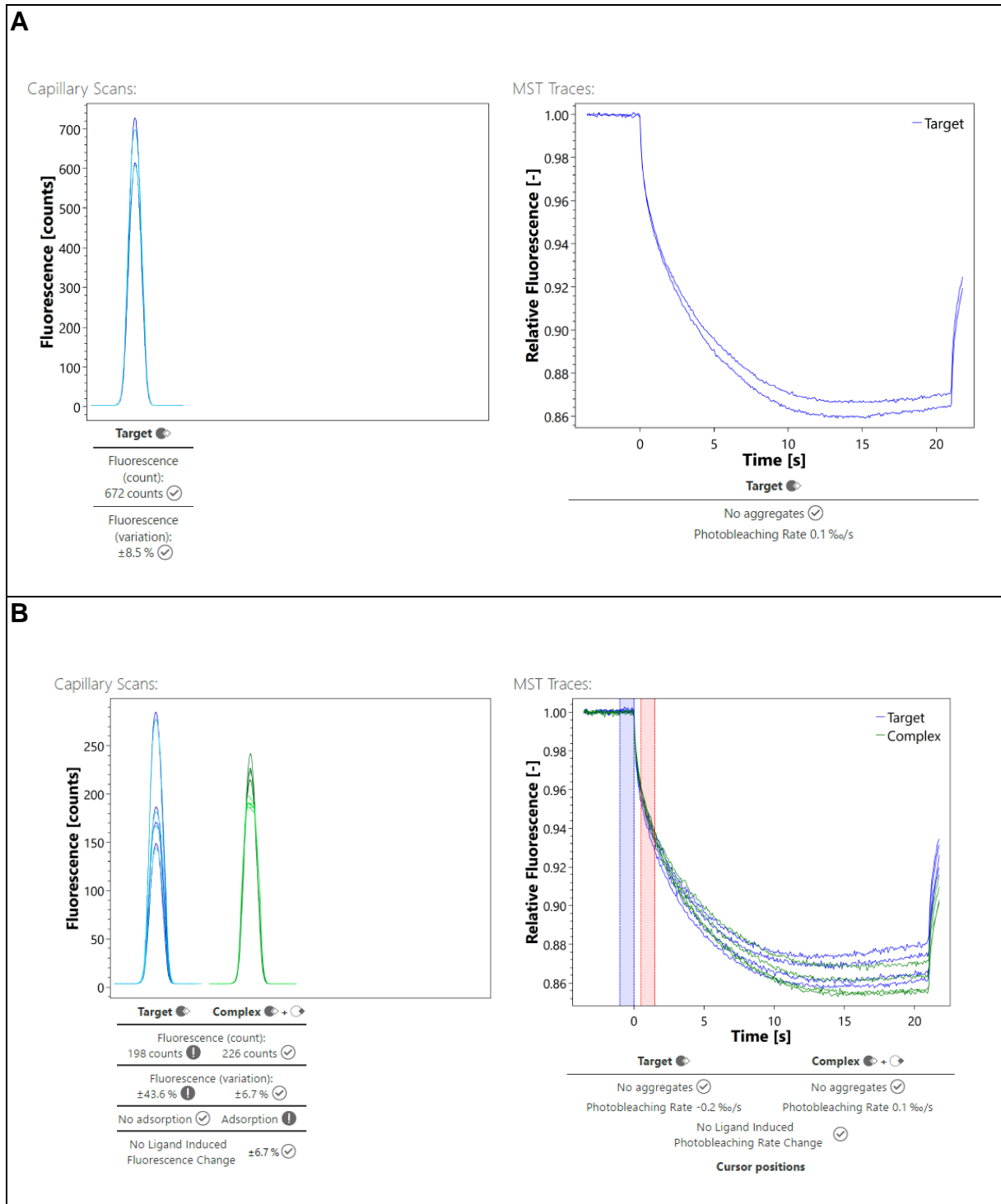


Figure 13: A) Pretest of *SmdHODH* sample in absence of ligands for Micro Scale Thermophoresis (MST). The non-significant variation of the MST profile in the experiment for the pure protein indicates the success in protein labelling. **B)** Binding check for *SmdHODH* and compound 0320. The MST profile indicates a variation of the relative fluorescence, indicating, a non-homogeneous behavior among the capillaries.

4.5. Structural analysis

The structural analysis was described in Mori *et al.*, 2020 (56), and its reproduction here was authorized by the John Wiley & Sons under the license number 5016010292565 (RightsLink®).

Crystallization assays were performed with pure and concentrated protein, using the sitting drop method. The sparse-matrix method implemented in commercially available screening kits was used for the initial crystallization experiments. After finding the best crystallization condition in 0.1 M HEPES sodium pH 7.5, 1.4 M sodium citrate tribasic dihydrate (Crystal Screen 1, solution #38), it was optimized. Crystals were obtained (**Figure 14**) after the optimization using: 0.1 M MES pH 6.5, 1.3 – 1.5 M citrate; and 0.1 M HEPES sodium pH 7.5, 1.3 – 1.5M citrate.

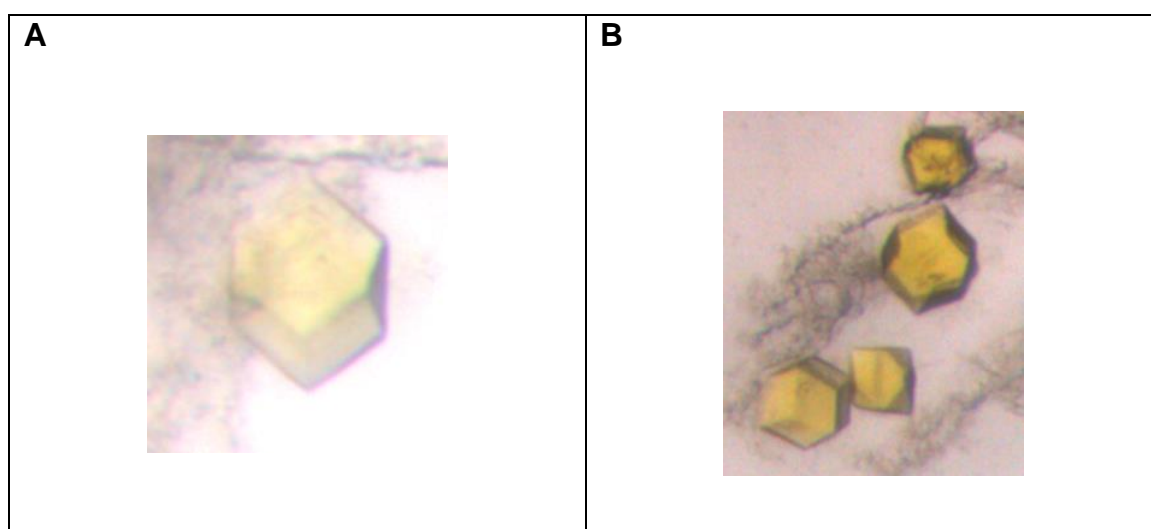


Figure 14: *SmDHODH* crystals obtained in A) 0.1 M MES pH 6.5, 1.3 – 1.5 M citrate; and B) 0.1 M HEPES sodium pH 7.5, 1.3 – 1.5M citrate.

The crystal structure of *SmDHODH* was solved by X-ray diffraction to 2.8 Å resolution (PDB ID: **6UY4**), in complex with the inhibitor 2-((4-fluorophenyl)amino)-3-hydroxynaphthalene-1,4-dione (0230) (56). The 0230 is a simplified hydroxynaphthoquinone analogue of atovaquone (**Figure 7**), with lower lipophilicity and lower molecular weight, containing an amino group as a spacer between the fluorophenyl ring and the quinone core.

4.5.1. Overall structure

The asymmetric unit contains the truncated construct that encompasses residues from Leu²³ to Ser³⁷⁹ presented as a monomer. Due to the lack of interpretable electron

density, three residues (23, 24, and 379) were excluded from the crystallographic structure model. The final structure contains one polypeptide chain, one FMN, four glycerol molecules, 64 solvent sites treated as water oxygens, and one 0230 compound. The crystallographic data were summarized in **Table 3**.

Table 3: Data collection and refinement statistics. (Extracted from Mori,R.M. et al. (56)).

Data collection	
Beamline	Proxima 2 (SOLEIL)
Space group	I 4 3 2
Cell dimensions	
<i>a, b, c</i> (Å)	187.98, 187.98, 187.98
α, β, γ (°)	90, 90, 90
Resolution range (Å)	47.00 – 2.80 (2.95 – 2.80)
CC1/2	0.997 (0.404)
<i>I</i> / σ (<i>I</i>)	15.2 (1.0)
Completeness (%)	99.8 % (99.2%)
Multiplicity	39.8 (40.1)
Refinement	
Resolution (Å)	2.80
No. reflections	14,308
$R_{\text{work}}/R_{\text{free}}$	0.217/0.246
Total number of atoms	2738
Average <i>B</i> -factors, all atoms (Å ²)	79.9
R.m.s. deviations	
<i>Bond lengths</i> (Å)	0.002
<i>Bond angles</i> (°)	0.479
Ramachandran plot	
Favored (%)	95.45%
Allowed (%)	4.55%

Statistics for the highest-resolution shell are shown in parentheses.

The structure comprises two main domains linked by an extended loop: the N-terminal alpha-helical domain and the α/β barrel domain where the active site is located (**Figure 15**). The central barrel is formed by eight parallel β strands ($\beta 1$ – $\beta 8$) surrounded by eight α -helices ($\alpha 1$ – $\alpha 8$). Sealing the bottom of the barrel, there are two antiparallel β strands (βA – βB). Between the top of the barrel and a subdomain composed by loops and the secondary structural elements βC , βD and βE , is placed the prosthetic group FMN. The helices αA and αB constitute the N-terminal alpha-helical domain, creating a hydrophobic channel that leads to the active site and has been identified as the binding site for class 2 inhibitors, as atovaquone and its analogues, including 0230.

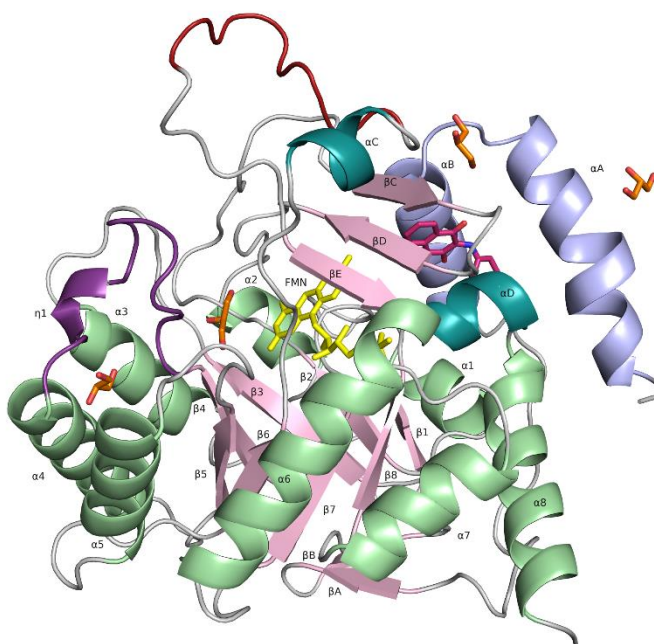


Figure 15: *SmDHODH* crystallographic structure represented by cartoon. The central barrel is composed of eight parallel β strands ($\beta 1$ – $\beta 8$) in lightpink and surrounded by eight α -helices in green ($\alpha 1$ – $\alpha 8$). The hydrophobic N-terminal domain composed by two α -helices is illustrated in lightblue (αA and αB). The catalytic loop (Asn²⁰⁰ – Lys²¹⁵) is highlighted in violet, and the protuberant loop (Gly²⁸⁵ – Lys²⁹⁴) in red. The glycerol molecules, the compound 0230, and the FMN are illustrated by stick models in orange, magenta, and yellow, respectively (Extracted from Mori,R.M. *et al.*, 2020 (56)).

4.5.2. Catalytic loop

The called catalytic loop orchestrates the dihydroorotate access and the orotate release by a dynamic process in the active site. In all another class 2 DHODHs crystal structures available in the protein data bank (PDB), it was found in its closed and active conformation (regardless of the presence of orotic acid). However, in the *SmDHODH* crystal structure, it is possible to observe this loop in an open conformation (**Figure**

16). Analyzing a structural superposition between *Sm*DHODH and the class 2 DHODH structures from *Homo sapiens* (*Hs*DHODH), *Plasmodium falciparum* (*Pf*DHODH), and *Mycobacterium tuberculosis* (*Mt*DHODH) it is possible to observe this opening of the active site loop in the schistosome structure, and a structural rearrangement of the region (**Figure 15**). In the DHODH from *S. mansoni*, the region that encompasses from the Asn²⁰⁰ to Lys²¹⁵, connecting the elements α 4 and β 4 (**Figure 6, Figure 15**), shows a long disordered region (Asn²⁰⁰ to Leu²⁰⁹) followed by a short 3_{10} helix (Arg²¹⁰ to Leu²¹²). On the other hand, in its closed conformation, the disordered region is shorter (Asn²¹² to Gly²²⁰ in human DHODH) and an alpha helix (Leu²²¹ to Gln²²⁵ in human DHODH) is present. In light of the high sequence identity noticed in this region (**Figure 6**), it is feasible to speculate whether the opening of the catalytic loop associated with the loss in alpha-helical content is a general feature shared by class 2 DHODHs and mandatory for catalysis.

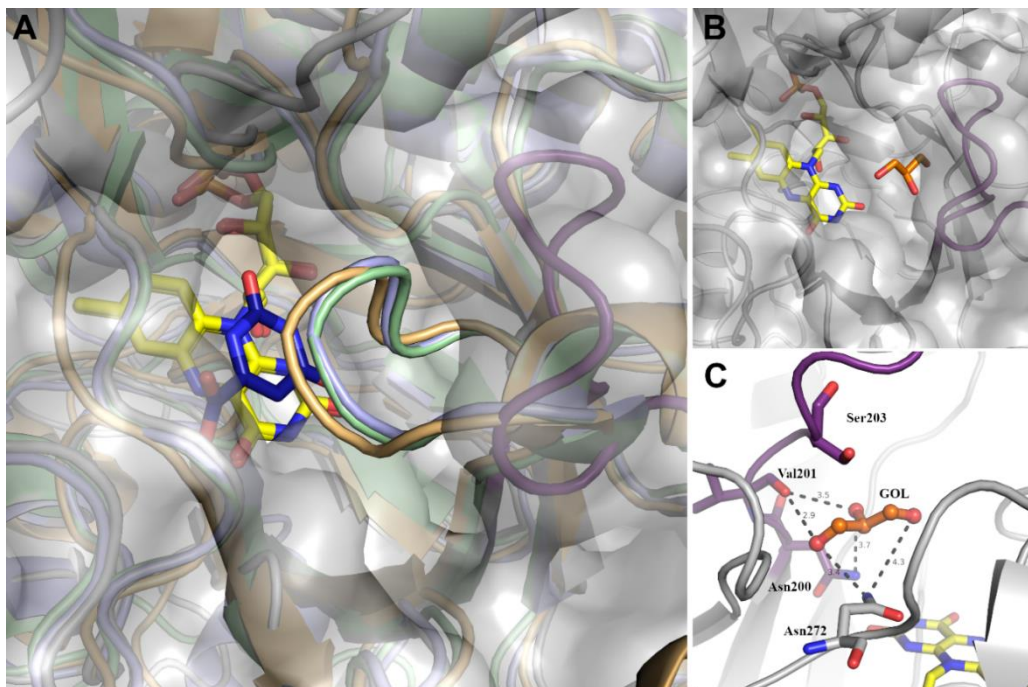


Figure 16: (A) Superposition between *Sm*DHODH and *Pf*DHODH (PDB: 1TV5; (88)), *Hs*DHODH (PDB: 1D3H; (89)), and *Mt*DHODH (PDB: 4XQ6; not published) showing the catalytic loop conformational rearrangement (Asn²⁰⁰ – Lys²¹⁵). Molecular surface for the *Sm*DHODH is represented in gray. The *Sm*DHODH, *Hs*DHODH, *Pf*DHODH, and *Mt*DHODH catalytic loop is colored in purple, lightblue, palegreen, and lightorange, respectively. The orotate and FMN are represented by stick models in blue and yellow, respectively. (B) *Sm*DHODH surface with a glycerol molecule at the entrance of the active site represented as stick model in orange (C) Glycerol molecule interactions (Extracted from Mori, R.M. *et al.*, 2020 (56)).

At the entrance of the active site, a glycerol molecule is present when the loop is found in its open conformation (**Figure 16B**). It is not clear if the glycerol only

interacts with the loop in its open-state configuration or induces its opening. Nevertheless, the glycerol is stabilized by hydrophobic interactions with the fully conserved residues Asn²⁰⁰, Val²⁰¹, Asn²⁷², and the catalytic base Ser²⁰³, and coordinates a complex hydrogen-bond network (O2 from glycerol and N δ_2 /Asn²⁰⁰, O2, and O3 from glycerol and C=O from Val²⁰¹ and O3 from glycerol and N δ_2 /Asn²⁷²) (**Figure 16C**).

The glycerol binding highlights new opportunities for class 2 DHODH drug discovery. Occluding the access to the active site (**Figure 16B**), molecules could retain the catalytic loop movement with the adequate stereo- and chemical properties, blocking the access of the substrates, hence interfering with enzymatic function. Moreover, mapping of the dihydroorotate/orotate binding pocket in FTmap for the identification of hot spots (90) unveiled an expressive gain of interior surface area comparing the open (*Sm*DHODH) and closed (*Hs*DHODH, PDBID: **1D3H**) states (2430 Å² and 1120 Å², respectively). With this, the opening of the catalytic loop in the schistosome structure reveals a new druggable pocket that could be broadly used in the design of DHODH inhibitors.

By reason of the advent of resistance for DHODH inhibitors that occupy the ubiquinone binding site, a new mode of class 2 DHODHs inhibition is a particular interest of the scientific community (91). Several features as the sequence and structural similarity of the active site shared by class 2 DHODHs, the expected similar mechanism of catalysis, associated with its biological role, highlight that this singular and transient druggable pocket presented for the first time in the *Sm*DHODH-0230 complex crystal structure, could be used in class 2 DHODH-based drug discovery projects as a strategy to overcome drug resistance.

4.5.3. Protuberant domain

The *S. mansoni* DHODH displays a 10-residue insertion (Gly²⁸⁵ to Lys²⁹⁴) that links β_6 and β_E structural elements (**Figure 15**). Interestingly, this protuberant domain is found highly conserved in all species from the genus *Schistosoma*, and absent in another class 2 DHODH deposited (**Figure 6**). It consists of a alpha helix α_C (Tyr²⁷⁸ to Val²⁸²), and by a loop solvent-exposed that antecedes the β_E strand (**Figure 15**) (68), allowing a significant rearrangement in this region compared to other structures.

Based on this, in previous experiments, Calil, F.A. (84) design a *SmDHODH* Δ loop construct, where the fragment between Gly²⁸⁵ to Lys²⁹⁴ was deleted. This construct shared similar circular dichroism (CD) spectra with *SmDHODH*. CD experiments are used to evaluate protein stability and secondary structure content. Therefore, the spectra obtained indicates that *SmDHODH* Δ loop maintains its structural integrity, once that a similar secondary structure distribution was observed for both constructs. However, *SmDHODH* Δ loop construct did not exhibit any enzymatic activity compared to the full length enzyme (56) (**Figure 17**).

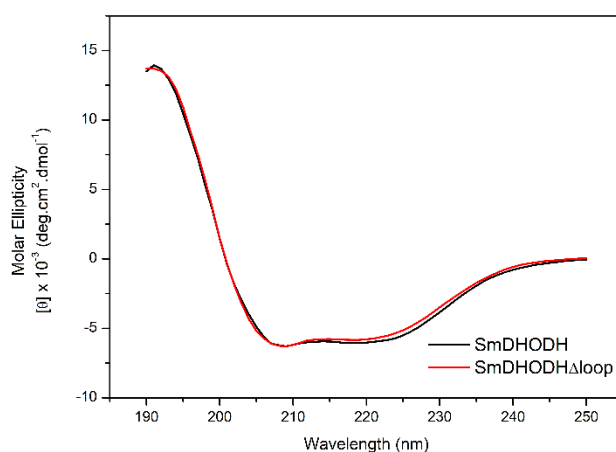


Figure 17: Circular dichroism spectra for both constructs: full-length (*SmDHODH*) and with the protuberant domain deleted (*SmDHODH* Δ loop), indicating the same secondary structure distribution. The graph represents the molar ellipticity per wavelength, where the full-length construct spectra is represented in black and the Δ loop spectra in red (Extracted from Mori, RM. *et al.*, 2020 (56)).

The effect of the removal of this protuberant domain in inhibitor binding was investigated by ThermoFMN experiments performed using both constructs. A comparison on the thermal stability effects with IC_{50} against a library of atovaquone-analogues was performed (56, 92) (**Figure 8, Figure 18**).

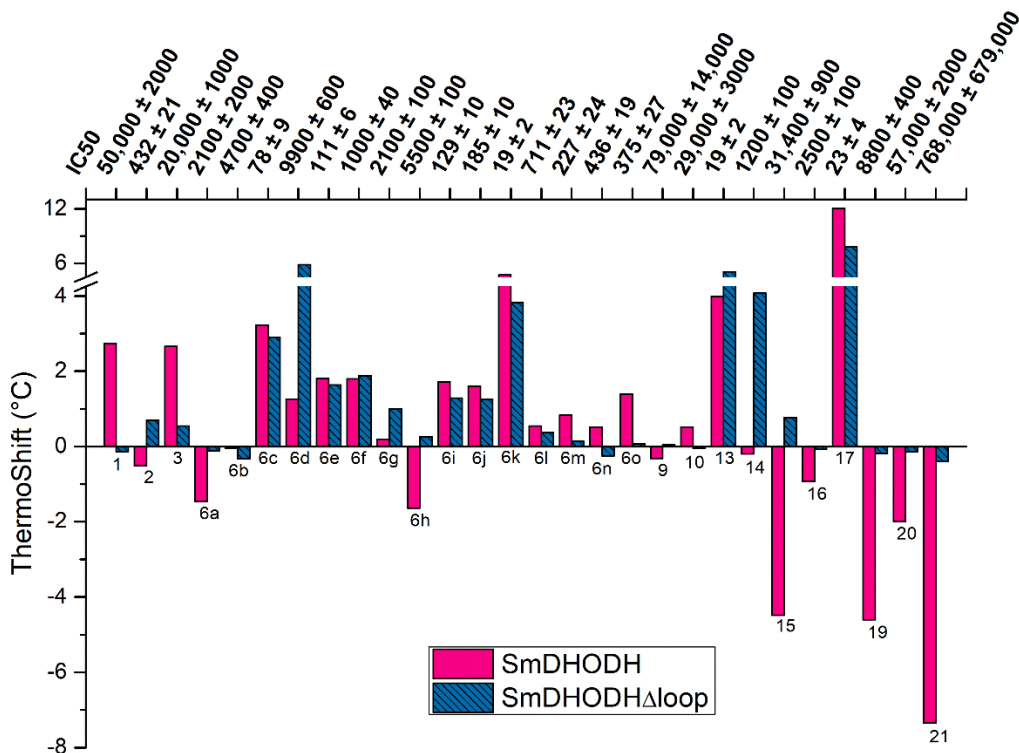


Figure 18: Graphic of inhibition values vs. ΔT_m shifts for the tested library at 500 μ M against *Schistosoma mansoni* dihydroorotate dehydrogenases: *SmDHODH* (full-length) and *SmDHODH Δ loop*. References T_m s are 54.73 $^{\circ}$ C for *SmDHODH* and 50.4 $^{\circ}$ C for *SmDHODH Δ loop*. IC₅₀ values were extracted from Calil *et al.* (92). (Extracted from Mori, RM. *et al.* (56)).

Similar to what has been described in the topic 4.3 for the fragments, we have investigated a correlation between enzymatic inhibition assays and ThermoFMN experiments of potent compounds from the atovaquone analogs library (IC₅₀ between 19 nM to \sim 1 μ M) - including 0230 (6f). Compounds with inhibition mode related to 0230 (6c, 6e, 6f, 6i, 6j, 6k, 6l, 6m, 6n, 13, 17) produced potency-dependent thermal shift trendlines for both constructs (**Figure 8, Figure 18**). It is possible to observe a slightly larger thermo shift towards the *SmDHODH* construct, indicating that removal of the protuberant loop interferes with protein-ligand interaction.

The oxidant agent Q₀, the coenzyme used in our enzymatic assays (**Figure 8**), binds to *SmDHODH* favoring the FMN release ($\Delta T_m = -6^{\circ}$ C), possibly due to its role in enzyme kinetics, inducing the opening of the catalytic loop. Thus, inhibitors that resemble it, as the compounds 19 to 21, display similar large negative thermal profile against the full-length construct (**Figure 18**). However, no significant thermal shift was observed for these molecules when tested against the *SmDHODH Δ loop*, indicating

that removal of the protuberant domain destabilizes the quinone binding site, and explains the lack of enzymatic activity observed for *Sm*DHODH Δ loop.

A distinct thermal stabilization profile is also observed for 6d and 14, comparing the constructs (**Figure 18**). Due to their high IC₅₀ and low binding strength, the slight thermal shift observed for *Sm*DHODH was expected (**Figure 18**). However, a very noticeable stabilizing effect towards *Sm*DHODH Δ loop was noticed for these compounds (**Figure 18**).

These peculiar thermo shift behaviors of compounds that interact with the quinone binding site between the constructs can indicate that the protuberant domain influences directly on the arrangement of the inhibitor binding site, and its removal can enhance or disfavor interactions.

Little is known about the catalytic mechanism adopted by this class of enzyme. But our results can help to identify potential druggable pockets in the protein. Analyzing the lack of ability of *Sm*DHODH Δ loop to interact with Q₀ reinforce a possible crosstalk between subdomains and its relationship with the catalytic mechanism, and the role of this connecting domain in class 2 DHODHs.

Previously, our group described a possible correlation between the mechanism of action and thermo stability (84). It was hypothesized that compounds that display competitive mechanism of inhibition could bind to the end of binding site channel, and mimic the interaction between the FMN and quinone, inducing the opening of the active site loop, exposing the flavin and favoring its release, and, consequently, displaying a negative thermo shift. On the other hand, compounds identified as non-competitive displayed positive thermal shifts, probably indicating their inability to reach the pocket end, binding to the channel beginning, stabilizing the structure, and avoiding the FMN release. However, the co-crystallized compound 0230 (6f) binds at the very end of the binding pocket (described below) and presents a positive thermo shift. Removal of the protuberant domain has indicated a crosstalk between subdomains in the protein. With this, the entrance of small compounds, similar to quinone (19 to 21), can really mimic the substrate effects on protein stability, as hypothesized in these previous studies from our group, and described in our results above. But, not necessarily, based on the crystal structure, compounds that bind to the channel end induce the active site loop opening. Therefore, probably each compound has a propensity to bind to a more or

less stable protein conformation. The behavior observed for 6d and 14 can corroborate this idea, once that even in a conformation where the quinone binding site is destabilized (*Sm*DHODH Δ loop), they were able to promote a large positive thermal shift, that is, they were able to bind and protect this construct from an early thermal denaturation, what did not happen with the full-length construct.

4.5.4. Inhibitor binding-site

*Sm*DHODH crystals were obtained in complex with 0230, a simplified analog of atovaquone, and previously identified as *Sm*DHODH inhibitor (92) (**Figure 19**).

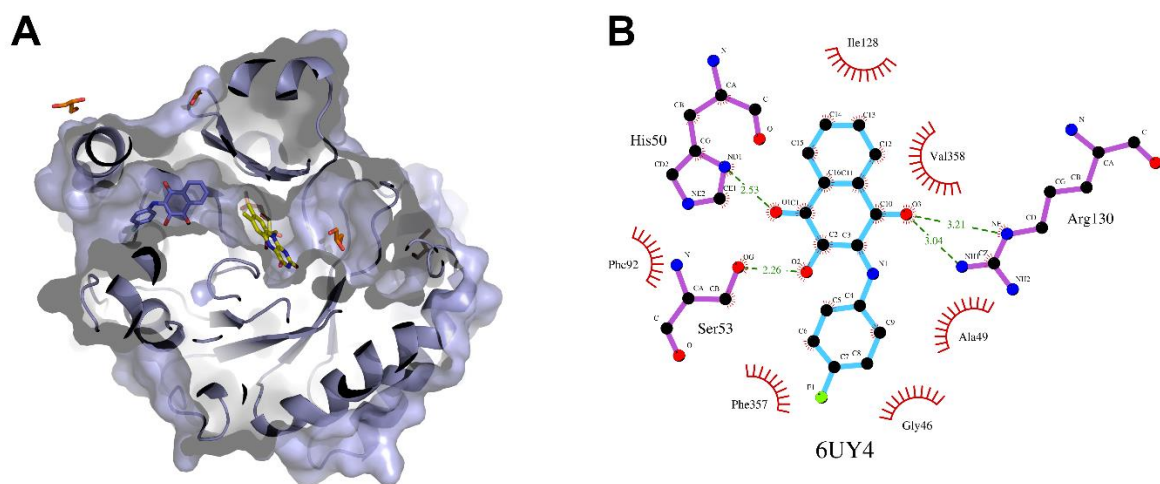


Figure 19: (A) *Schistosoma mansoni* dihydroorotate dehydrogenase (*Sm*DHODH; PDBID: 6UY4) molecular surface and cartoon representation. Represented by sticks: 0230 (2-((4-fluorophenyl) amino)-3-hydroxynaphthalene-1,4-dione) in blue, FMN in yellow and glycerol molecules in green. Image created with PyMOL (82). (B) Schematic interactions in the complex 0230-*Sm*DHODH. C, N, O and F atoms are shown in black, blue, red and lime green, respectively. The green dashed lines represent the hydrogen bonds. Image created with LIGPLOT+ (93). (Extracted from Mori, RM. et al. (56)).

The two V-shaped α helices (α A e α B) that compose the N-terminal domain were found to be the binding site for all class 2 DHODH inhibitors, including atovaquone (94), teriflunomide and brequinar (89), similar to what is observed for 0230 (**Figure 8**, **Figure 18A**).

Figure 19B illustrates the overall binding of the complex 0230-*Sm*DHODH. The compound interacts with residues coming from the helix α B from the N-terminus helical domain, α D - that connects β 8 and α 8, the loop connecting β 1 and α 1, and β C from the top of the barrel. Specifically, 0230 interacts with the protein through hydrogen bonds with the residues: His⁵⁰, Ser⁵³, and Arg¹³⁰ (His⁵⁰ and Arg¹³⁰ are fully conserved

among class 2 DHODHs (**Figure 6**), and play an important role in inhibitor binding), and hydrophobic interactions with Gly⁴⁶, Ala⁴⁹, Phe⁹², Ile¹²⁸, Phe³⁵⁷, and Val³⁵⁸ (**Figure 19B**).

Unexpected results about the 0230-binding mode can be observed. Structural comparison between the complexes 0230-*Sm*DHODH and atovaquone-*Rn*DHODH (rat DHODH; PDBID:1UUM; (94)) revealed that the hydroxynaphthoquinone moiety of 0230 underwent a 180° rotation along the N1-C3 bond (**Figure 19, Figure 20**). A carbonyl group of the quinoidal ring forms a cyclic hydrogen-bonded system with the conserved Arg¹³⁰ (Arg¹³⁶ in *Hs*DHODH) (N ϵ and NH1 from Arg¹³⁰ and C10=O3 from 0230). With this, the opposite carbonyl group can be stabilized by the His⁵⁰ via an additional hydrogen-bond (N δ from His⁵⁰ and C1=O1 from 0230). This flipped conformation for the hydroxynaphthoquinone portion is favored by the presence of the Ser⁵³, conserved among *Schistosoma* spp., and substituted by Ala⁵⁹ in human and rat DHODHs (**Figure 6**). Compared to the *Hs*DHODH, the Ser⁵³, which stabilizes the hydroxynaphthoquinone moiety by a hydrogen-bond with its hydroxyl group (O γ from Ser⁵³ and O2 from 0230), contributes to generate a more polar environment in the parasitic DHODH. This serine's presence seems to influence the inhibition, since substitutions in the hydroxyl group reflect on a low inhibitory activity (**Figure 8, Figure 18**) (92). For example, the polar nature of Ser⁵³ pushes away the fluorophenyl ring from the 0230 towards the helix α A.

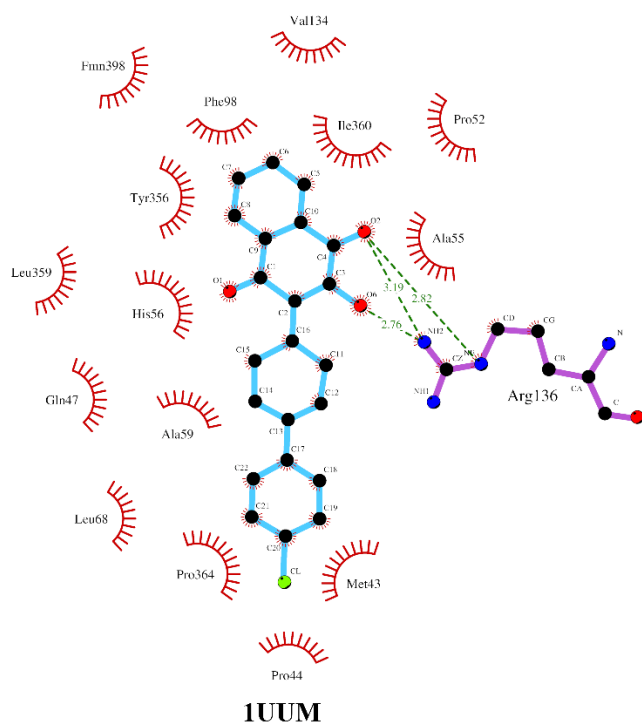


Figure 20: Schematic interactions in the complex atovaquone-*RnDHODH* (PDID: 1UUM). C, N, O and F atoms are shown in black, blue, red and lime green, respectively. The green dashed lines represent the hydrogen bonds. Image created with LIGPLOT+ (93). (Extracted from Mori, RM. et al. (56)).

To avoid a steric clash against the α A helix when bound to *SmDHODH*, the atovaquone (ATO) requires a large structural rearrangement, in consideration of the same flipped configuration would be observed for its hydroxynaphthoquinone head. The freedom of ATO to rotate along the C2-C16 bond allied to the structural flexibility of its cyclohexane ring, allows that this could be achieved chemically.

Finally, an overall analysis of the previously tested library (92) and of the fragments reported in the topic 4.2 and 4.3 suggests that the atovaquone scaffold is essential for inhibition and is the most promising strategy for drug design against the ubiquinone binding site. With exception of the compound 0320, the another five fragments with significative inhibition data follow this chemical structure. From the atovaquone analogs library is possible to stablish correlations that will be useful for future drug optimization. We clustered the library in two groups according to their chemical features. Firstly, the 0230-like compounds are simplified analogs of atovaquone (6a – 6k), the presence of a NH-spacer group influences their mobility, tolerating the molecules to adopt different arrangements, hence, promoting new

interactions by additional hydrogen bonds, changing the electron density distribution of both quinone and phenyl rings. The pattern of substitution of the phenyl ring affects the structural organization of the ligand: i) *ortho*-substituted phenyl rings have limited flexibility compared to those with *meta*- and *para*-substitutions. However, the presence of a halogen on lipophilicity, conformation, and non-covalent interactions, can overcome this pattern, once that the most active compound in this 0230-like series contains an *o-m*-dichloro-substituted phenyl ring (6k); ii) larger benzo-fused heterocycles (6g and 6h) and *o-o*-disubstituted phenyl ring (6d) indicating higher molecular volume and steric hindrance for adopting bioactive conformation, respectively, affecting the ideal complementarity. The role of lipophilicity and conformation can be observed also for lapachol (13) and reduced lapachol (17), with acyclic and apolar substitution to the hydroxynaphthoquinone core. The second group is the atovaquone-like series (6l - 6o) with a bioisosteric substitution of the cyclohexane to piperazine. It has increased polarity and reduced lipophilicity without changing conformational properties. This series showed similar activity to atovaquone (2) suggesting the same type of molecular interactions with the parasitic enzyme (**Figure 8, Figure 18**). In this sense, the absence of a halogen group at the fragment 0009 can explain the results found in the ThermoFMN assays (**Figure 11**), as well the best values of IC₅₀ for the other 0230-like compounds (0011, 0034 and 0297), as described before. Taken into account all analysis performed with both libraries, it is possible to conclude that the differential thermal stabilization profile can be also attributed to combined effects on conformation, lipophilicity, and non-covalent interactions, due to the absence of the halogen, since the inhibitors that displayed positive thermal shifts contains at least one halogen group. Besides that, the halogen type also seems to be important, since the substitution of the fluorine for a chlorine (0230 and 0011, respectively) increased the potency more than ten times.

Structurally, important amino acid substitutions can be highlighted as responsible for creating a distinct environment in the inhibitor binding pocket compared to the human enzyme. For example, at the entrance of the inhibitor binding site, Ala³⁹ and Leu⁵⁶ in *SmdHODH* are replaced by Leu⁴⁶ and Phe⁶² in *HsDHODH*, respectively. Moreover, modifications such as Phe³⁵ (replaced by Leu⁴² in *HsDHODH*), Leu³⁶ (Met⁴³), Ala³⁹ (Leu⁴⁶), Arg⁴⁰ (Gln⁴⁷), Gly⁴⁶ (Pro⁵²), Ala⁵⁷ (Thr⁶³), Ile⁶² (Leu⁶⁸), Ile¹²⁸ (Val¹³⁴), Phe³⁵⁷ (Leu³⁵⁹) and Val³⁵⁸ (Thr³⁶⁰) contribute in substantial differences in terms

of chemical, steric, and dynamic properties to be widely exploited for fragments optimization.

5. CONCLUSION

The present work describes the search for new selective inhibitors against *SmDHODH* by target-based approaches, focused on the use of fragment-screening combining a multidisciplinary approach. Several molecules with a broad range of scaffolds were tested and evaluated against *SmDHODH*. With this, using biophysical and biochemical evaluations we identified potent ligands/inhibitors. We have described the analysis of the first crystal structure of *SmDHODH* in complex with the inhibitor (2-((4-fluorophenyl)amino)-3-hydroxynaphthalene-1,4-dione. Our findings can represent a milestone in the search for class 2 DHODH inhibitors. First, the structure provides key insights into how this enzyme is regulated (catalytic loop and protuberant domain). Second, the transient druggable pocket described can be widely used in future class 2 DHODH-based drug discovery projects. Finally, our work shows key molecular interactions required for the activity of atovaquone and its analogues that allied with the fragments analysis presented can guide future drug design strategies in the fight against this prevalent NTD.

6. REFERENCES

1. Food and Drug Administration F. [Available from: <https://www.fda.gov/patients/drug-development-process/step-1-discovery-and-development>.
2. Mikulic M. Total global spending on pharmaceutical research and development from 2012 to 2026: Statista; 2020 [Available from: <https://www.statista.com/statistics/309466/global-r-and-d-expenditure-for-pharmaceuticals/>.
3. DiMasi JA. Assessing Pharmaceutical Research and Development Costs. *JAMA Internal Medicine*. 2018;178(4):587-.
4. Mohs RC, Greig NH. Drug discovery and development: Role of basic biological research. *Alzheimer's & dementia (New York, N Y)*. 2017;3(4):651-7.
5. Swinney D. Phenotypic vs. target-based drug discovery for first-in-class medicines. *Clinical Pharmacology & Therapeutics*. 2013;93(4):299-301.
6. Moffat JG, Vincent F, Lee JA, Eder J, Prunotto M. Opportunities and challenges in phenotypic drug discovery: an industry perspective. *Nature Reviews Drug Discovery*. 2017;16(8):531-43.
7. Aulner N, Danckaert A, Ihm J, Shum D, Shorte SL. Next-Generation Phenotypic Screening in Early Drug Discovery for Infectious Diseases. *Trends in Parasitology*. 2019;35(7):559-70.
8. Drews J. Drug Discovery: A Historical Perspective. *Science*. 2000;287(5460):1960.
9. Croston GE. The utility of target-based discovery. *Expert Opinion on Drug Discovery*. 2017;12(5):427-9.

10. Sams-Dodd F. Target-based drug discovery: is something wrong? *Drug Discovery Today*. 2005;10(2):139-47.
11. Kirsch P, Hartman AM, Hirsch AKH, Empting M. Concepts and Core Principles of Fragment-Based Drug Design. *Molecules* (Basel, Switzerland). 2019;24(23):4309.
12. Shepherd CA, Hopkins AL, Navratilova I. Fragment screening by SPR and advanced application to GPCRs. *Progress in Biophysics and Molecular Biology*. 2014;116(2):113-23.
13. Pollack SJ, Beyer KS, Lock C, Müller I, Sheppard D, Lipkin M, et al. A comparative study of fragment screening methods on the p38 α kinase: new methods, new insights. *Journal of computer-aided molecular design*. 2011;25(7):677-87.
14. Hopkins AI, Groom CR, Groom Cr, Alex A, Alex A. Ligand efficiency: a useful metric for lead selection. (1359-6446 (Print)).
15. Hoelz LVB, Calil FA, Nonato MC, Pinheiro LCS, Boechat N. Plasmodium falciparum dihydroorotate dehydrogenase: a drug target against malaria. *Future Medicinal Chemistry*. 2018;10(15):1853-74.
16. Eder J, Sedrani R, Wiesmann C. The discovery of first-in-class drugs: origins and evolution. *Nat Rev Drug Discov*. 13. England 2014. p. 577-87.
17. Gilbert IH. Drug Discovery for Neglected Diseases: Molecular Target-Based and Phenotypic Approaches. *Journal of Medicinal Chemistry*. 2013;56(20):7719-26.
18. Organization WH. Neglected tropical diseases [Available from: https://www.who.int/neglected_diseases/en/].
19. Hotez PJ, Alvarado M, Basáñez M-G, Bolliger I, Bourne R, Boussinesq M, et al. The Global Burden of Disease Study 2010: Interpretation and Implications for the Neglected Tropical Diseases. *PLOS Neglected Tropical Diseases*. 2014;8(7):e2865.
20. Nelwan ML. Schistosomiasis: Life Cycle, Diagnosis, and Control. *Current Therapeutic Research*. 2019;91:5-9.
21. Organization WH. Schistosomiasis - Fact sheet. 2018.
22. Martins DdS, Xavier MF, Masiero FdS, Cordeiro J, Thyssen PJ. Schistosomiasis in Southern Brazil 17 years after the confirmation of the first autochthonous case. *Revista da Sociedade Brasileira de Medicina Tropical*. 2015;48:354-7.
23. Saúde Md. Esquistossomose: causas, sintomas, tratamento, diagnóstico e prevenção [Available from: <http://www.saude.gov.br/saude-de-a-z/esquistossomose>].
24. Bizimana P, Ortu G, Van Geertruyden J-P, Nsabiyumva F, Nkeshimana A, Muhimpundu E, et al. Integration of schistosomiasis control activities within the primary health care system: a critical review. *Parasites & Vectors*. 2019;12(1):393.
25. Nascimento GL, Pegado HM, Domingues ALC, Ximenes RAdA, Itria A, Cruz LN, et al. The cost of a disease targeted for elimination in Brazil: the case of schistosomiasis mansoni. *Memórias do Instituto Oswaldo Cruz*. 2019;114.
26. McManus DP, Dunne DW, Sacko M, Utzinger J, Vennervald BJ, Zhou X-N. - Schistosomiasis. 2018;- 4(- 1).
27. Centers for Disease Control and Prevention [Available from: <https://www.cdc.gov/>].
28. Cardoso IA. Structural and biochemical characterization of Schistosoma mansoni class II fumarate hydratase enzyme.
29. Gray DJ, Ross AG, Li Y-S, McManus DP. Diagnosis and management of schistosomiasis. *Bmj*. 2011;342:d2651.
30. Lima CWR, Oliveira NMCd, Silva SVDd, Duarte MEL, Barbosa APF. Ectopic forms of schistosomiasis mansoni in the second macroregion of Alagoas: case series report and review of the literature. *Revista da Sociedade Brasileira de Medicina Tropical*. 2017;50:812-8.
31. Coyle CM, Garcia HH, Tanowitz HB, Del Brutto OH. Chapter 22 - Schistosomiasis of the nervous system. *Handbook of Clinical Neurology*. 114: Elsevier; 2013. p. 271-81.
32. Mickael CS, Graham BB. The Role of Type 2 Inflammation in Schistosoma-Induced Pulmonary Hypertension. *Frontiers in Immunology*. 2019;10(27).
33. Kamath N, Iyengar A. Infections and the kidney: a tale from the tropics. *Pediatric Nephrology*. 2018;33(8):1317-26.

34. Siqueira LdP, Fontes DAF, Aguilera CSB, Timóteo TRR, Ângelos MA, Silva LCPBB, et al. Schistosomiasis: Drugs used and treatment strategies. *Acta Tropica*. 2017;176:179-87.
35. Cioli D, Pica-Mattoccia L, Basso A, Guidi A. Schistosomiasis control: praziquantel forever? *Molecular and Biochemical Parasitology*. 2014;195(1):23-9.
36. Ismail M, Metwally A, Farghaly A, Bruce J, Tao L-F, Bennett JL. Characterization of Isolates of *Schistosoma mansoni* from Egyptian Villagers that Tolerate High Doses of Praziquantel. *The American Journal of Tropical Medicine and Hygiene*. 1996;55(2):214-8.
37. Stelma FF, Talla I, Sow S, Kongs A, Niang M, Polman K, et al. Efficacy and Side Effects of Praziquantel in an Epidemic Focus of *Schistosoma mansoni*. *The American Journal of Tropical Medicine and Hygiene*. 1995;53(2):167-70.
38. Andrews P, Thomas H, Pohlke R, Seubert J. Praziquantel. *Medicinal Research Reviews*. 1983;3(2):147-200.
39. Vale N, Gouveia MJ, Rinaldi G, Brindley PJ, Gärtner F, Correia da Costa JM. Praziquantel for Schistosomiasis: Single-Drug Metabolism Revisited, Mode of Action, and Resistance. *Antimicrobial Agents and Chemotherapy*. 2017;61(5):e02582-16.
40. Meyer T, Sekljic H, Fuchs S, Bothe H, Schollmeyer D, Miculka C. Taste, A New Incentive to Switch to (R)-Praziquantel in Schistosomiasis Treatment. *PLoS Neglected Tropical Diseases*. 2009;3(1):e357.
41. Doenhoff MJ, Cioli D, Utzinger J. Praziquantel: mechanisms of action, resistance and new derivatives for schistosomiasis. *Current opinion in infectious diseases*. 2008;21(6):659-67.
42. Pax R, Bennett J, Fetterer R. A benzodiazepine derivative and praziquantel: effects on musculature of *Schistosoma mansoni* and *Schistosoma japonicum*. *Naunyn-Schmiedeberg's archives of pharmacology*. 1978;304(3):309-15.
43. Kohn A, Roberts-Misterly J, Anderson P, Khan N, Greenberg R. Specific sites in the beta interaction domain of a schistosome Ca²⁺ channel β subunit are key to its role in sensitivity to the anti-schistosomal drug praziquantel. *Parasitology*. 2003;127(4):349-56.
44. Park SK, Gunaratne GS, Chulkov EG, Moehring F, McCusker P, Dosa PI, et al. The anthelmintic drug praziquantel activates a schistosome transient receptor potential channel. *J Biol Chem*. 2019;294(49):18873-80.
45. Thomas CM, Timson DJ. The *Schistosoma mansoni* tegumental allergen protein, SmTAL1: Binding to an IQ-motif from a voltage-gated ion channel and effects of praziquantel. *Cell Calcium*. 2020;86:102161.
46. Timson DJ. Praziquantel: An Enigmatic, Yet Effective, Drug. *Methods Mol Biol*. 2020;2151:1-8.
47. Mo AX, Agosti JM, Walson JL, Hall BF, Gordon L. Schistosomiasis elimination strategies and potential role of a vaccine in achieving global health goals. *Am J Trop Med Hyg*. 2014;90(1):54-60.
48. Beniguel L, Diallo TO, Remoue F, Williams DL, Cognasse F, Charrier-Mze N, et al. Differential production in vitro of antigen specific IgG1, IgG3 and IgA: a study in *Schistosoma haematobium* infected individuals. *Parasite Immunol*. 2003;25(1):39-44.
49. Riveau G, Deplanque D, Remoue F, Schacht AM, Vodougnon H, Capron M, et al. Safety and immunogenicity of rSh28GST antigen in humans: phase 1 randomized clinical study of a vaccine candidate against urinary schistosomiasis. *PLoS Negl Trop Dis*. 2012;6(7):e1704.
50. Tran MH, Pearson MS, Bethony JM, Smyth DJ, Jones MK, Duke M, et al. Tetraspanins on the surface of *Schistosoma mansoni* are protective antigens against schistosomiasis. *Nat Med*. 2006;12(7):835-40.
51. Hotez PJ, Bethony JM, Diemert DJ, Pearson M, Loukas A. Developing vaccines to combat hookworm infection and intestinal schistosomiasis. *Nat Rev Microbiol*. 2010;8(11):814-26.
52. Tandler M, Almeida M, Vilar M, Pinto P, Limaverde-Sousa G. Current status of the Sm14/GLA-SE Schistosomiasis vaccine: overcoming barriers and paradigms towards the first

- anti-parasitic Human (itarian) vaccine. *Tropical medicine and infectious disease*. 2018;3(4):121.
53. Inobaya MT, Olveda RM, Chau TN, Olveda DU, Ross AG. Prevention and control of schistosomiasis: a current perspective. *Research and reports in tropical medicine*. 2014;2014(5):65-75.
 54. Fenwick A, Webster JP, Bosque-Oliva E, Blair L, Fleming FM, Zhang Y, et al. - The Schistosomiasis Control Initiative (SCI): rationale, development and implementation from 2002–2008. 2009;- 136(- 13).
 55. Caffrey CR, El-Sakkary N, Mäder P, Krieg R, Becker K, Schlitzer M, et al. Drug Discovery and Development for Schistosomiasis. *Neglected Tropical Diseases*. 2019:187-225.
 56. de Mori RM, Aleixo MAA, Zapata LCC, Calil FA, Emery FS, Nonato MC. Structural basis for the function and inhibition of dihydroorotate dehydrogenase from *Schistosoma mansoni*. *The FEBS Journal*. 2020;n/a(n/a).
 57. Reis RAG, Calil FA, Feliciano PR, Pinheiro MP, Nonato MC. The dihydroorotate dehydrogenases: Past and present. *Archives of Biochemistry and Biophysics*. 2017;632:175-91.
 58. Hoelz LV, Calil FA, Nonato MC, Pinheiro LC, Boechat N. Plasmodium falciparum dihydroorotate dehydrogenase: a drug target against malaria. *Future Med Chem*. 2018;10(15):1853-74.
 59. Pinheiro MP, Emery FdS, Cristina Nonato M. Target Sites for the Design of Anti-trypanosomatid Drugs Based on the Structure of Dihydroorotate Dehydrogenase. *Current Pharmaceutical Design*. 2013;19(14):2615-27.
 60. Madak JT, Bankhead A, 3rd, Cuthbertson CR, Showalter HD, Neamati N. Revisiting the role of dihydroorotate dehydrogenase as a therapeutic target for cancer. *Pharmacol Ther*. 2019;195:111-31.
 61. Sykes DB. The emergence of dihydroorotate dehydrogenase (DHODH) as a therapeutic target in acute myeloid leukemia. *Expert Opin Ther Targets*. 2018;22(11):893-8.
 62. Oliver JD, Sibley GE, Beckmann N, Dobb KS, Slater MJ, McEntee L, et al. F901318 represents a novel class of antifungal drug that inhibits dihydroorotate dehydrogenase. *Proc Natl Acad Sci U S A*. 2016.
 63. Cordeiro AT, Feliciano PR, Pinheiro MP, Cristina Nonato M. Crystal structure of dihydroorotate dehydrogenase from *Leishmania major*. *Biochimie*. 2012;94(8):1739-48.
 64. Lucas-Hourani M, Dauzonne D, Jorda P, Cousin G, Lupan A, Helynck O, et al. Inhibition of pyrimidine biosynthesis pathway suppresses viral growth through innate immunity. *PLoS Pathog*. 2013;9(10):e1003678.
 65. Fang J, Uchiumi T, Yagi M, Matsumoto S, Amamoto R, Takazaki S, et al. Dihydroorotate dehydrogenase is physically associated with the respiratory complex and its loss leads to mitochondrial dysfunction. *Biosci Rep*. 2013;33(2):e00021.
 66. Gattermann N, Dadak M, Hofhaus G, Wulfert M, Berneburg M, Loeffler ML, et al. Severe impairment of nucleotide synthesis through inhibition of mitochondrial respiration. *Nucleosides Nucleotides Nucleic Acids*. 2004;23(8-9):1275-9.
 67. Löffler M, Carrey EA, Zameitat E. Orotate (orotic acid): An essential and versatile molecule. *Nucleosides, Nucleotides & Nucleic Acids*. 2016;35(10-12):566-77.
 68. Nonato MC, de Pádua RAP, David JS, Reis RAG, Tomaleri GP, D'Muniz Pereira H, et al. Structural basis for the design of selective inhibitors for *Schistosoma mansoni* dihydroorotate dehydrogenase. *Biochimie*. 2019;158:180-90.
 69. Corpet F. Multiple sequence alignment with hierarchical clustering. *Nucleic Acids Research*. 1988;16(22):10881-90.
 70. Robert X, Gouet P. Deciphering key features in protein structures with the new ENDscript server. *Nucleic Acids Research*. 2014;42(W1):W320-W4.
 71. Liu S, Neidhardt EA, Grossman TH, Ocain T, Clardy J. Structures of human dihydroorotate dehydrogenase in complex with antiproliferative agents. *Structure*. 2000;8(1):25-33.

72. Davies M, Heikkilä T, McConkey GA, Fishwick CWG, Parsons MR, Johnson AP. Structure-Based Design, Synthesis, and Characterization of Inhibitors of Human and Plasmodium falciparum Dihydroorotate Dehydrogenases. *Journal of Medicinal Chemistry*. 2009;52(9):2683-93.
73. Singh A, Maqbool M, Mobashir M, Hoda N. Dihydroorotate dehydrogenase: A drug target for the development of antimalarials. *European Journal of Medicinal Chemistry*. 2017;125:640-51.
74. Calil FA, David JS, Chiappetta ERC, Fumagalli F, Mello RB, Leite FHA, et al. Ligand-based design, synthesis and biochemical evaluation of potent and selective inhibitors of Schistosoma mansoni dihydroorotate dehydrogenase. *European Journal of Medicinal Chemistry*. 2019;167:357-66.
75. Kabsch W. Xds. *Acta Crystallographica Section D-Biological Crystallography*. 2010;66:125-32.
76. Winn MD, Ballard CC, Cowtan KD, Dodson EJ, Emsley P, Evans PR, et al. Overview of the CCP4 suite and current developments. *Acta Crystallographica Section D*. 2011;67(4):235-42.
77. McCoy AJ, Grosse-Kunstleve RW, Adams PD, Winn MD, Storoni LC, Read RJ. Phaser crystallographic software. *Journal of applied crystallography*. 2007;40(Pt 4):658-74.
78. Adams PD, Afonine PV, Bunkoczi G, Chen VB, Davis IW, Echols N, et al. PHENIX: a comprehensive Python-based system for macromolecular structure solution. *Acta Crystallographica Section D*. 2010;66(2):213-21.
79. Afonine PV, Grosse-Kunstleve RW, Echols N, Headd JJ, Moriarty NW, Mustyakimov M, et al. Towards automated crystallographic structure refinement with phenix.refine. *Acta Crystallographica Section D*. 2012;68(4):352-67.
80. Emsley P, Lohkamp B, Scott WG, Cowtan K. Features and development of Coot. *Acta Crystallographica Section D*. 2010;66(4):486-501.
81. Chen VB, Arendall WB, III, Headd JJ, Keedy DA, Immormino RM, Kapral GJ, et al. MolProbity: all-atom structure validation for macromolecular crystallography. *Acta Crystallographica Section D*. 2010;66(1):12-21.
82. Schrodinger L. The PyMOL molecular graphics system, version 1.8. Schrodinger LLC, New York, NY. 2015.
83. Pádua RAP, Tomaleri GP, Reis RAG, David JS, Silva VC, Pinheiro MP, et al. ThermoFMN - a thermofluor assay developed for ligand-screening as an alternative strategy for drug discovery. *Journal of the Brazilian Chemical Society*. 2014;25:1864-71.
84. Calil FA, Nonato MC. Repurposing of antimalarial drugs in the treatment of schistosomiasis based on the selective inhibition of the enzyme dihydroorotate dehydrogenase. 2019.
85. Reis RA, Ferreira P, Medina M, Nonato MC. The mechanistic study of Leishmania major dihydro-orotate dehydrogenase based on steady- and pre-steady-state kinetic analysis. *Biochem J*. 2016;473(5):651-60.
86. Rainard JM, Pandarakalam GC, McElroy SP. Using Microscale Thermophoresis to Characterize Hits from High-Throughput Screening: A European Lead Factory Perspective. *SLAS discovery : advancing life sciences R & D*. 2018;23(3):225-41.
87. Entzian C, Schubert T. Studying small molecule-aptamer interactions using MicroScale Thermophoresis (MST). *Methods*. 2016;97:27-34.
88. Hurt DE, Widom J, Clardy J. Structure of Plasmodium falciparum dihydroorotate dehydrogenase with a bound inhibitor. *Acta Crystallographica Section D-Biological Crystallography*. 2006;62:312-23.
89. Liu SP, Neidhardt EA, Grossman TH, Ocain T, Clardy J. Structures of human dihydroorotate dehydrogenase in complex with antiproliferative agents. *Structure with Folding & Design*. 2000;8(1):25-33.
90. Kozakov D, Grove LE, Hall DR, Bohnuud T, Mottarella SE, Luo L, et al. The FTMap family of web servers for determining and characterizing ligand-binding hot spots of proteins. *Nat Protoc*. 2015;10(5):733-55.

91. Ross LS, Gamo FJ, Lafuente-Monasterio MJ, Singh OM, Rowland P, Wiegand RC, et al. In vitro resistance selections for *Plasmodium falciparum* dihydroorotate dehydrogenase inhibitors give mutants with multiple point mutations in the drug-binding site and altered growth. *J Biol Chem*. 2014;289(26):17980-95.
92. Calil FA, David JS, Chiappetta ERC, Fumagalli F, Mello RB, Leite FHA, et al. Ligand-based design, synthesis and biochemical evaluation of potent and selective inhibitors of *Schistosoma mansoni* dihydroorotate dehydrogenase. *Eur J Med Chem*. 2019;167:357-66.
93. Laskowski RA, Swindells MB. LigPlot+: multiple ligand-protein interaction diagrams for drug discovery. *J Chem Inf Model*. 2011;51(10):2778-86.
94. Hansen M, Le Nours J, Johansson E, Antal T, Ullrich A, Loffler M, et al. Inhibitor binding in a class 2 dihydroorotate dehydrogenase causes variations in the membrane-associated N-terminal domain. *Protein Science*. 2004;13(4):1031-42.

APPENDICES

Figures S1 to S6. Graphs showing the log of the inhibitor concentration versus the percent of inhibition, for obtaining the compounds IC_{50} against *SmdHODH*.

